https://doi.org/10.5194/egusphere-2026-4927
Preprint. Discussion started: 27 August 2026

Respiration depth and the conditional diffusive oxygen supply to the Bay of Bengal oxygen minimum zone: a one-dimensional model

Khandaker Estiyak Zaman Turjo[1], Sumit Sarker[2], S M Mahatab Uddin[3], Tajrian Meem Bithi[2], Arnab Naha Ushna[4], Mohammad Abdul Momin Siddique[3,5,*]

[1]Department of Marine Sciences, University of Georgia, Athens, Georgia 30602-3636, USA
[2]Department of Oceanography, Noakhali Science and Technology University, Noakhali 3814, Bangladesh
[3]Department of Oceanography and Coastal Sciences, Louisiana State University, Baton Rouge, Louisiana, USA
[4]Department of Civil Engineering, Bangladesh University of Engineering and Technology (BUET), Dhaka 1000, Bangladesh
[5]University of South Bohemia in České Budějovice, Faculty of Fisheries and Protection of Waters, South Bohemian Research Center of Aquaculture and Biodiversity of Hydrocenoses, Vodňany 38925, Czech Republic

[*]Correspondence: siddique.ocn@nstu.edu.bd (Mohammad Abdul Momin Siddique)

Abstract. The oxygen balance of an oxygen minimum zone (OMZ) reflects competition between respiratory consumption of sinking organic matter and physical resupply. How much organic matter is respired has received far more attention than where it is respired, yet that depth determines whether the demand acts on the OMZ core or the oxygenated water above it. This study quantifies the control with a one-dimensional offline plankton–oxygen model at five Bay of Bengal stations spanning a sevenfold range of core oxygen, perturbing the detrital sinking speed and remineralisation rate with every budget closed from recorded increments. Moving from the weak-transfer to the baseline configuration displaces respiratory demand downward and increases it eightfold to thirteenfold within a baseline-defined core layer. The resulting loss of oxygen contrast across the core upper interface reduces the downward diffusive supply by -37 to -9 %, with the larger responses in the three oxygen-depleted columns. That amplitude is set by prescribed closures rather than by the particle physics, spanning -14 to -48 % across perturbations of vertical diffusivity, restoring timescale, oxygen half-saturation and diagnostic layer width. It survives removing oxygen restoring from the upper 50 m but collapses, and at one station reverses, when the upper 100 m is freed: the response requires that the water above the core not deoxygenate with it. At one station, configurations sharing a constant ratio of the two parameters agree to about 1 % across the tested triplet, so oxygen alone separates them poorly over that range. Independent biogeochemical Argo float profiles, used for evaluation only, place the modelled oxycline in the same 25 m bin as the observed one and reproduce the station ordering of core oxygen, but do not constrain the interface gradient, which varies by more than a factor of two between defensible processing choices. The mechanism therefore remains untested against observations.

Keywords: Oxygen minimum zone; Particle remineralisation; Respiratory oxygen demand; Vertical oxygen diffusion; Bay of Bengal

https://doi.org/10.5194/egusphere-2026-4927
Preprint. Discussion started: 27 August 2026

1. Introduction

Oxygen minimum zones (OMZs) occupy a small fraction of the ocean volume but exert a disproportionate influence on nitrogen cycling, habitat compression and trace-metal chemistry (Stramma et al., 2008; Levin et al., 2009; Paulmier and Ruiz-Pino, 2009). Observational and model syntheses indicate that oceanic oxygen has declined over recent decades and that OMZs have expanded (Schmidtko et al., 2017; Breitburg et al., 2018; Oschlies et al., 2018). Their persistence reflects a local competition between respiratory consumption of sinking organic matter and physical resupply of oxygen. Where that balance leaves oxygen close to suboxia, small changes in either term alter the partition between oxic remineralisation and denitrification, and therefore the rate at which fixed nitrogen is removed from the ocean (Codispoti et al., 2001; Devol, 2008; DeVries et al., 2012).

The Bay of Bengal occupies an unusual position in this respect. Its OMZ is among the shallowest in the world ocean, yet core oxygen concentrations remain a few micromolar above the level at which canonical denitrification becomes widespread, and measured N_2 production is correspondingly limited by nitrite availability rather than by oxygen alone (Naqvi et al., 2006; Naqvi et al., 2010; Bristow et al., 2017). Freshwater discharge from the Ganges–Brahmaputra–Meghna system and heavy monsoonal rainfall maintain a strong near-surface halocline that suppresses vertical exchange, most severely in the north (Shetye et al., 1991; Vinayachandran et al., 2002; Sengupta et al., 2006). Oxygen supply to the thermocline is correspondingly multidimensional: seasonal and intraseasonal circulation, the monsoon current system and mesoscale features all contribute (Vinayachandran et al., 2004; Wiggert et al., 2006; Resplandy et al., 2009; Vinayachandran et al., 2013). These physical pathways are increasingly well constrained. The response of the *local* oxygen balance to a change in where particle-derived respiratory demand is imposed is far less resolved.

Particle flux attenuates with depth, and that attenuation is conventionally summarised by an empirical power-law transfer profile (Martin et al., 1987; Buesseler et al., 2007). Such profiles

https://doi.org/10.5194/egusphere-2026-4927
Preprint. Discussion started: 27 August 2026

describe how much organic matter survives to a given depth, but the biogeochemical consequence depends on the depth at which the surviving material is respired. Kwon et al. (2009) showed that shifting the global remineralisation depth alters the air–sea carbon balance substantially even when export production is held fixed, establishing the depth of respiration as a control distinct from its magnitude. Attenuation is itself not a fixed property. It varies with temperature (Marsay et al., 2015), and the settling behaviour that sets it emerges from aggregation, fragmentation and grazing acting on a diverse particle population rather than from any single sinking velocity (Stemmann et al., 2004; Boyd and Trull, 2007). A closely related demonstration exists for the oxygen budget itself. Bianchi et al. (2013) found that vertically migrating animals, by carrying organic matter below the euphotic zone before respiring it, intensify open-ocean oxygen depletion at depth. The transport mechanism there is active rather than passive, but the principle is the same: relocating respiration in the vertical changes the oxygen field even when the total is unchanged. It has received comparatively little attention for the passive particle flux in a shallow OMZ, where the respiratory demand and the oxygen minimum are separated by only tens of metres.

A deliberately reduced framework suits this question. A one-dimensional model resolves the vertical diffusion operator explicitly, permits controlled perturbation of the particle field, and allows every term of the local oxygen budget to be recorded as the increment its operator actually applies, so that realised respiratory demand, resolved diffusive supply and the residual required to close the budget are separated without reconstruction. Because the vertical diffusivity is prescribed rather than solved, any change in the diffusive flux across a fixed interface is attributable entirely to a change in the modelled oxygen gradient, which is precisely the quantity a redistribution of respiratory demand is expected to alter. The cost is equally explicit: horizontal advection and eddy transport are absent, so the residual is a closure quantity rather than an estimate of any particular circulation pathway, and the vertical mixing that sets

https://doi.org/10.5194/egusphere-2026-4927
Preprint. Discussion started: 27 August 2026

the amplitude of the diffusive response is imposed rather than constrained by regional turbulence measurements. A second difficulty concerns parameter identification. Sinking speed and remineralisation rate together set an effective attenuation length, so where the oxygen response is governed mainly by that combination the two are poorly distinguished, and a calibration that adjusts one while holding the other fixed may locate an apparent optimum that reflects that choice rather than the data. Concerns that plankton models carry more adjustable parameters than the available constraints can determine are long-standing (Oschlies, 2001; Anderson, 2005).

The analysis presented here quantifies how the detrital sinking speed and remineralisation rate redistribute potential and realised respiratory oxygen demand around a fixed, baseline-defined core layer, and determines the accompanying change in core oxygen structure and in the resolved vertical diffusive supply across the core upper interface. Five stations whose forcing supports the diagnostic core, spanning a sevenfold range of background core oxygen, establish how far the response depends on oxygen state rather than on the particle perturbation alone. Configurations sharing a constant ratio of sinking speed to remineralisation rate test whether the two parameters are separately identifiable from the oxygen response. The vertical diffusivity and the restoring timescale, the two prescribed quantities that most directly set the core budget, are varied to establish which features of the response are structural and which belong to the baseline physics. The vertical extent over which oxygen is restored is varied in the same way, which turns out to bound the result rather than merely scale it. Finally, the modelled oxygen structure is compared with BGC-Argo profiles that play no part in constructing or constraining the model. The scope throughout is the local vertical balance at five stations; no estimate of basin-scale ventilation is attempted.

https://doi.org/10.5194/egusphere-2026-4927
Preprint. Discussion started: 27 August 2026

2. Materials and Methods

2.1 Study area

The Bay of Bengal occupies the northeastern Indian Ocean and is bounded to the north and west by the Indian subcontinent (Fig. 1a). Discharge from the Ganges–Brahmaputra–Meghna system, together with heavy monsoonal rainfall, produces a strong and persistent near-surface salinity stratification that is most pronounced in the north and weakens southward (Shetye et al., 1991; Vinayachandran et al., 2002). This stratification limits the vertical exchange of oxygen between the surface mixed layer and the thermocline.

The quantitative analysis uses the five stations at which both forcing products carry data through the diagnostic core: S2 on the northern slope, S3 and S4 in the central and western central bay, S5 in the more oxygenated south, and S6 on the Andaman side (Table 1). They were chosen to span a wide range of background oxygen states rather than to sample a continuous geographical section, and they do: baseline annual-mean core oxygen ranges from 3.00 mmol m^{-3} at S2 to 20.3 mmol m^{-3} at S5, a factor of seven, with oxygen minima at different depths (Fig. 1b). S2 is the most depleted column of the six and S5 the best ventilated.

The experimental coverage is not uniform across the five, and the asymmetry is stated here rather than left to be inferred from the tables. All five carry the weak and baseline particle configurations, which is the pair the core-budget comparison rests on. The extended parameter matrix, comprising the high, isolation, near-neutral, intermediate-high and constant-ratio configurations, is concentrated at S3 and S4, the two central stations where the mechanism is diagnosed in detail; S5 additionally carries the high and isolation configurations, and legacy S1 integrations are retained only as forcing-limited numerical and context diagnostics. Table 2 lists which configurations were integrated at which station.

S1 is excluded from the quantitative analysis, and the reason is a property of the forcing rather than of the results. Its position on the Ganges–Brahmaputra shelf and upper slope means that neither product carries data through the model domain: GLORYS12 temperature ends at

https://doi.org/10.5194/egusphere-2026-4927
Preprint. Discussion started: 27 August 2026

77.9 m and WOA23 oxygen at 125 m, below which the station input file is filled by constant downward extrapolation (Table 1). Sparse subsurface sampling is a general feature of this part of the basin rather than a peculiarity of these two products (Masud-Ul-Alam et al., 2026). The S1 diagnostic core spans 95–200 m, so 30 m of its 105 m integrated thickness is observationally supported and 75 m, or 71 %, is fill. Every core-integrated quantity at S1 is therefore dominated by an extrapolated value, and none is used here. S1 is retained on the station map and in the Supplement as a numerical-closure test and as a demonstration of what an unsupported column produces; the common 1000 m domain is physically supported at S2–S6 only. The five analysed stations are not treated as a transect and no property section is constructed between them.

2.2 Model framework

The model is a one-dimensional offline NPZD–O_2 formulation of the type introduced by Fasham et al. (1990), extended with prognostic oxygen and a denitrifying remineralisation pathway. *Offline* means that no momentum or circulation equations are solved: there is no horizontal advection, no geostrophic adjustment and no resolved mesoscale transport. The vertical diffusivity and the surface atmospheric forcing are prescribed externally. Temperature and salinity are prognostic scalar arrays, advanced each step by the same implicit vertical diffusion operator applied to the tracers and then relaxed toward monthly climatological profiles on a 30-day timescale; they are therefore numerically integrated, but they are constrained to follow a prescribed climatology rather than evolving freely. The biogeochemical tracers are advanced under that prescribed and nudged physical state.

Boundary conditions are as follows. All tracers, including temperature and salinity, have zero diffusive flux at the surface and at 1000 m. Detritus leaves the domain through the bottom face at its sinking velocity and enters through no face at the surface. Oxygen exchanges with the atmosphere through the surface cell by Eq. (7) alone; the diffusive surface flux is zero.

https://doi.org/10.5194/egusphere-2026-4927
Preprint. Discussion started: 27 August 2026

The vertical domain spans 0–1000 m with N = 200 uniform levels of thickness Δz = 5 m, giving cell centres at 2.5–997.5 m. The physical time step is 1 h, and the biological source–sink terms are advanced with 20 sub-steps per physical step. The model uses a 360-day calendar of twelve 30-day months, and all annual quantities in this paper refer to that calendar. Configuration details are collected in Table 2a and the complete parameter set in Tables S1 and S2.

Within each physical step, the operators are applied in the order: forcing update; temperature and salinity relaxation with vertical diffusion; nitrate restoring; oxygen restoring; vertical diffusion of the biogeochemical tracers; and biology, which includes detrital sinking and air–sea gas exchange. Vertical diffusion is solved implicitly with a tridiagonal solver. The biological update treats each sink term semi-implicitly in the first-order Patankar form $X^{n+1} = (X^n + \Delta t\, S)/(1 + \Delta t\, L)$ (Patankar, 1980), where S and L are the production rate and the specific loss rate; this guarantees positivity for the nitrogen compartments. It is not the high-order conservative modified-Patankar discretisation of Burchard et al. (2003), and conservation is therefore verified diagnostically rather than assumed. Oxygen positivity is *not* guaranteed by construction, because the respiration term enters the numerator, and is instead monitored with an explicit clipping term that is retained in the budget identity and diagnosed as exactly zero in every run reported here. Operator details are given in Supplement Section S1.

2.3 State variables and biological formulation

The model carries five biogeochemical tracers: nitrate (NO_3), phytoplankton (P), zooplankton (Z), detritus (D) and dissolved oxygen (O_2), with all nitrogen-based tracers in mmol N m^{-3} and oxygen in mmol O_2 m^{-3}. Phytoplankton growth follows a multiplicative light and nitrate limitation with a temperature-dependent maximum rate; grazing follows a Michaelis–Menten formulation with assimilation efficiency γ_Z, the unassimilated fraction

https://doi.org/10.5194/egusphere-2026-4927
Preprint. Discussion started: 27 August 2026

entering the detrital pool. Light attenuation follows a discrete Beer–Lambert integral including self-shading. Parameter values are listed in Tables S1 and S2.

Detritus is remineralised along an oxic pathway at a temperature-dependent rate modulated by an oxygen limitation factor, and along a denitrifying pathway when oxygen is low. Writing the temperature-dependent reference rate as

$$r_{\mathrm{eff}}(z) = r_d \exp[\theta_D (T(z) - T_{\mathrm{ref}})], \quad (1)$$

where θ_D = 0.063 °C^{-1} is an exponential temperature sensitivity inherited from the model lineage rather than fitted here; it corresponds to a Q_{10} near 1.9. The functional form is defined in this study following the model lineage, the coefficient is not independently constrained here, and no measurement of the temperature dependence of detrital remineralisation is claimed in its support. The oxic remineralisation rate is $r_{eff}\, f_{O_2}$ with

$$f_{O_2} = \frac{O_2}{K_{O_2} + O_2}, \quad (2)$$

The half-saturation constant K_{O2} = 4 mmol m^{-3} is a prescribed model parameter, not an observationally constrained one, and because η depends on it directly its influence is tested explicitly rather than assumed. The corresponding oxygen sink is r_{on} times the remineralised nitrogen. The value $r_{on} = r_{op}$ = 8.625 is the classical Redfield -O_2:N ratio; Anderson (1995) derives a higher value of 10.6 from measured elemental composition, which is 1.23 times larger; at fixed oxygen state the conditional potential oxygen demand would scale by that factor. A fully coupled stoichiometric sensitivity, in which the altered demand feeds back on oxygen and hence on f_{O_2} and on the restoring term, was not performed. When oxygen is low the residual detrital demand is met by denitrification at a rate

$$R_{\mathrm{dn}} = r_{\mathrm{dn}}\, r_{\mathrm{eff}} \left(1 - f_{O_2}\right) \frac{\mathrm{NO_3}}{k_{\mathrm{NO_3}} + \mathrm{NO_3}}\, D, \quad (3)$$

Equation (3) is a simplified legacy closure carried forward from the model lineage; no published source for this exact form could be identified, and it is not claimed to represent

https://doi.org/10.5194/egusphere-2026-4927
Preprint. Discussion started: 27 August 2026

observed water-column denitrification. The oxic and denitrifying branches together define the model detrital remineralisation rate, but they do not form exact complementary partitions, because the denitrifying branch carries both the scaling r_{dn} and a nitrate limiter that the oxic branch does not. Each mole of nitrogen remineralised along this pathway consumes r_{denit} moles of nitrate. Denitrification consumes no oxygen and therefore does not enter Eq. (8); its response to particle transport is reported in the Supplement.

A distinction that is central to this paper is that between the demand particles *could* exert and the demand they *do* exert. Equations (4) and (5) below are diagnostics defined in this study rather than model equations taken from the literature; they are evaluated online alongside the prognostic terms and never fed back into the model state. The conditional potential respiratory demand, meaning the instantaneous oxygen-unlimited sink evaluated at the realised detrital field, is obtained by setting f_{O_2} to 1,

$$A_{\mathrm{pot}}(z) = r_{\mathrm{on}}\, r_{\mathrm{eff}}(z)\, D(z), \tag{4}$$

and the realised demand $A_{act}(z)$ as the oxygen sink actually applied by the model, which includes both f_{O_2} and the implicit Patankar update. Vertically integrating each over the fixed core gives $A_{core,pot}$ and $A_{core,act}$, and their ratio defines the oxygen limitation factor

$$\eta = \frac{A_{\mathrm{core,act}}}{A_{\mathrm{core,pot}}}, \tag{5}$$

a ratio defined in this study. A_{pot} is a diagnostic evaluated with the same detrital field as the realised term; it is recorded online and never fed back into the model state.

Since A_{act} and A_{pot} differ only by f_{O_2} and the implicit update factor, η is exactly an A_{pot}-weighted mean of the prescribed Michaelis–Menten factor over the core. Evaluated across all twenty converged configurations, η equals that weighted mean to within 0.5 % and equals f_{O_2} evaluated at the core-mean oxygen concentration to within 0.026. η is therefore a compact diagnostic of how far the core sits down a prescribed limitation curve whose shape is fixed by

https://doi.org/10.5194/egusphere-2026-4927
Preprint. Discussion started: 27 August 2026

the single constant K_{O_2}; it is not an emergent relationship, and its numerical value is only as constrained as K_{O_2} is. What the experiments contribute is how far the modelled state moves along that curve when demand is redistributed, and how that displacement survives changing K_{O_2}.

A second structural consequence follows from Eq. (3). Because the oxic and denitrifying pathways carry rate coefficients $r_{eff}\, f_{O_2}$ and $r_{dn}\, r_{eff}(1-f_{O_2})g_{NO_3}$ with $r_{dn} = 1$ and $g_{NO_3} = 0.967$–0.984 over the analysed cores, their sum is 0.990–0.998 times r_{eff}. Total detrital decay in this model is therefore oxygen independent to within 1 %, and particle attenuation length does not respond to the oxygen field. The observed enhancement of organic-matter preservation through oxygen minimum zones is consequently absent by construction, which is a limitation of direct relevance to a study of where respiration occurs. The same equation also uses the phytoplankton nitrate half-saturation k_{NO3} as the denitrification nitrate limiter; because nitrate is restored on a 60-day timescale and g_{NO_3} stays near saturation, this simplification has little effect on the oxygen budget, but it is a shared symbol for two physically distinct processes rather than a derived equality.

2.4 Detrital transport

Detritus sinks at a prescribed speed w_D, positive downward. Sinking is applied as a separate conservative flux operator using a total-variation-diminishing scheme with the van Leer limiter $\varphi(r) = (r + |r|)/(1 + |r|)$ (van Leer, 1974), rather than as a source–sink term inside the biological update.

An idealised benchmark motivates this choice. Advecting a Gaussian detrital pulse for 20 days with no biology and no physical diffusion, a first-order upwind discretisation broadens the pulse from $\sigma = 20.0$ m to 37.4 m, corresponding to an effective numerical diffusivity of 2.9×10^{-4} m^2 s^{-1}. That is 29 times the prescribed physical diffusivity over the analysed depth range, 1.0×10^{-5} m^2 s^{-1} (Eq. 6), so a first-order scheme would impose a spurious spreading of

https://doi.org/10.5194/egusphere-2026-4927
Preprint. Discussion started: 27 August 2026

the particle field larger than the physical mixing it competes with. The van Leer scheme broadens the same pulse only to 20.9 m, corresponding to 1.1×10^{-5} m^2 s^{-1}, which is comparable to, rather than negligible against, the prescribed physical value over the analysed range. Halving and doubling the physical time step changes the weak-to-baseline F_{top} response at S3 by 0.005 percentage points and the baseline core oxygen by 0.03 % (Table S17), so the response is not sensitive to the temporal discretisation. The 5 m vertical grid is fixed in the station forcing files and could not be varied without regenerating every model input from the source products, so vertical-resolution dependence is stated as a limitation rather than tested. Because this study perturbs the vertical distribution of particles deliberately, controlling this numerical artefact is a prerequisite rather than a refinement. Full benchmark values are in Table S6 and Fig. S5, and implementation details in Supplement Section S2.

2.5 Vertical diffusion and physical forcing

Vertical diffusivity K_z is not taken from a reanalysis mixing scheme. It is prescribed analytically from the mixed-layer depth,

$$K_z(z) = K_{\mathrm{bg}} + \tfrac{1}{2}\left(K_{\mathrm{ml}} - K_{\mathrm{bg}}\right)\left[1 - \tanh\left(\tfrac{z-h_{\mathrm{ml}}}{h_{\mathrm{tr}}}\right)\right], \quad (6)$$

with $K_{ml} = 10^{-3}$ m^2 s^{-1}, $K_{bg} = 10^{-5}$ m^2 s^{-1} and a transition thickness $h_{tr} = 10$ m. The only external input is the monthly mixed-layer depth h_{ml}, taken from the GLORYS12 reanalysis variable mlotst (Lellouche et al., 2021); no reanalysis diffusivity field is used, and GLORYS12 is not the source of K_z. Because h_{ml} ranges from 10.7 to 31.7 m across the six stations, K_z falls to within 5 % of K_{bg} by 60–70 m and equals 1.000×10^{-5} m^2 s^{-1} to machine precision at every depth below 150 m, in every month, at every station. The analysed upper layer and core therefore lie entirely within a single prescribed constant, and F_{top} is that constant multiplied by the modelled oxygen gradient. One consequence of keying K_z to a reanalysis mixed-layer depth should be stated: comparison of CTD and Argo profiles against reanalysis output in the northern

https://doi.org/10.5194/egusphere-2026-4927
Preprint. Discussion started: 27 August 2026

Bay of Bengal shows the reanalysis to overestimate mixed-layer depth and to smooth fine-scale near-surface structure (Masud-Ul-Alam et al., 2026), so the depth of the transition in Eq. (6) inherits that bias. Because the analysed layers sit far below the transition, where K_z equals its background value regardless, this affects the upper-ocean tendencies rather than the core budget itself. This is a strong assumption and it is the principal reason the amplitude of the diffusive response reported below is treated as configuration specific.

Temperature and salinity are relaxed toward the WOA23 monthly climatology (Locarnini et al., 2024; Reagan et al., 2024). Surface shortwave radiation and 10 m wind speed are taken from the ERA5 reanalysis (Hersbach et al., 2020). Forcing profiles and their seasonal cycles are shown in Fig. S1, and their provenance and processing in Table S9.

2.6 Air–sea oxygen exchange

The air–sea oxygen flux is $k_{pist}(O_{2,sat} - O_2)$, positive into the ocean, and is applied as a tendency on the surface cell,

$$\left.\frac{\partial O_2}{\partial t}\right|_{\mathrm{AS}} = \frac{k_{\mathrm{pist}}}{\Delta z_1}\left(O_{2,\mathrm{sat}} - O_2\right), \tag{7}$$

where the division by the surface-cell thickness converts the areal flux to a concentration tendency, and oxygen saturation follows Weiss (1970) using both temperature and salinity, and the piston velocity follows the Wanninkhof (2014) parameterisation, with the oxygen Schmidt number from Wanninkhof (1992). The piston velocity is evaluated in m s^{-1}, consistent with the second-based time step used throughout the implementation. No tuning multiplier is applied to the piston velocity.

2.7 Restoring and its interpretation

Dissolved oxygen and nitrate are relaxed toward the WOA23 monthly climatology (Garcia et al., 2024b; Garcia et al., 2024a) with timescales τ_{O2} = 365 d and τ_{NO3} = 60 d, applied over

https://doi.org/10.5194/egusphere-2026-4927
Preprint. Discussion started: 27 August 2026

the full water column. The oxygen relaxation contributes a term $R_{restore}$ to the local oxygen budget.

This term is a *parameterised representation of unresolved external exchange*. It absorbs whatever the one-dimensional framework does not resolve, which includes horizontal advective and eddy transport but also any systematic mismatch between the prescribed physics, the biological formulation and the reference climatology. It is a closure term for the model, not a measurement. Its sign and magnitude are therefore reported as a diagnostic of local imbalance. The term is not converted into a lateral oxygen flux, attributed to a named current system, or expressed as a percentage contribution to OMZ maintenance.

2.8 Experimental design

The two parameters governing particle attenuation, w_D and r_d, are perturbed in the configurations listed in Table 2b. The baseline uses $w_D = 10$ m d^{-1} and $r_d = 0.10$ d^{-1}. A weak-transfer configuration uses (5, 0.15) and a high-transfer configuration (20, 0.10). An additional case at (5, 0.10) isolates the effect of w_D at fixed r_d, and (8, 0.10) provides an intermediate point. The configuration (8, 0.10) is termed *intermediate-high* rather than strong because its converged core demand is lower than that of the baseline.

Three further configurations at S3, namely (5, 0.05), (10, 0.10) and (20, 0.20), share a constant ratio $w_D/r_d = 100$ and test whether the oxygen response is organised by that ratio. Because r_{eff} is temperature dependent (Eq. 1), a constant nominal ratio does not correspond to an exactly constant attenuation length, so any such degeneracy is expected to be approximate.

2.9 Convergence and diagnostic window

Simulations were integrated until the convergence criterion was satisfied and diagnosed over the subsequent complete 360-day model year. The criterion requires that the year-on-year change in each monitored quantity remains below tolerance for the final three consecutive complete model years of the integration, and it is applied simultaneously to layer-mean oxygen,

https://doi.org/10.5194/egusphere-2026-4927
Preprint. Discussion started: 27 August 2026

total nitrogen and each biological compartment. The tolerance is 0.05 mmol m^{-3} for layer-mean oxygen and a relative 10^{-3} of the initial inventory for total nitrogen and for each of P, Z and D. Only complete model years enter the test. All configurations satisfied it by model year four to six, the latest being the two S6 integrations (Fig. S3a). The magnitude of the core oxygen inventory tendency over the diagnostic year is 10^{-7}–10^{-5} mmol $m^{-2}d^{-1}$ in every case (Fig. S3b), so storage is negligible but is retained explicitly in the budget rather than assumed zero.

2.10 Fixed diagnostic geometry

For each station a *baseline-defined core layer* is defined as the set of grid cells whose centres fall within ±50 m of the converged baseline oxygen-minimum depth, and an upper layer as the immediately overlying 50 m. Both are specified as fixed cell-index ranges and are held constant across every particle-transport configuration at that station, so that responses are not contaminated by a diagnostic window that moves with the solution.

The ±50 m cell-centre rule selects 21 cells, giving an *integrated thickness of 105 m* bounded by interfaces rather than 100 m; at S3 and S4 the cell centres span 172.5–272.5 m and the bounding interfaces 170–275 m, and layer integrals use the interface bounds. The layer is a fixed *reference* interval defined once from the baseline state; it is not the instantaneous oxygen-minimum layer of every perturbation. At S4 under the weak configuration the global oxygen minimum lies at 362.5 m, below the baseline-defined core (Table S3). This does not affect the budget, which is closed over a fixed volume by construction, but it is the reason the term baseline-defined core layer is preferred to OMZ core when comparing configurations. The resulting geometry is given in Table 1 and Fig. 1c.

2.11 Exact online oxygen budget

Equations (8) and (9) are bookkeeping identities of this model's operator sequence, defined here rather than adopted from an external framework. Every oxygen source and sink is recorded

https://doi.org/10.5194/egusphere-2026-4927
Preprint. Discussion started: 27 August 2026

online as the actual increment applied by its operator, and accumulated over the same records used for the inventory change. The full identity for a layer is

$$\frac{dI}{dt} = P_{\mathrm{photo}} + R_{\mathrm{resp}} + A_{\mathrm{remin}} + F_{\mathrm{AS}} + R_{\mathrm{restore}} + B_{\mathrm{diff}} + C_{\mathrm{clip}}, \quad (8)$$

where I is the layer oxygen inventory and C_{clip} collects any positivity clipping. No term is reconstructed from saved mean fields.

In the S2–S6 cores the photosynthesis, respiration and air–sea terms are exact zeros, and Eq. (8) reduces to a balance between demand, diffusion and restoring. At S1 they are not zero, because the shallower oxygen minimum places the core closer to the euphotic zone; the reduced form leaves a residual there some eight orders of magnitude larger than the full form (Fig. S4c). All S1 diagnostics therefore use the complete seven-term identity.

Diffusive fluxes at layer interfaces are reconstructed exactly from the recorded cell-wise increments. With no diffusive flux through the surface, the downward flux at interface j is $F_j = -\sum_{k<j} G_k$, where G_k is the net diffusive gain of cell k. The net resolved diffusive supply to a layer bounded by interfaces j_{top} and j_{bot} is then

$$B_{\mathrm{diff}} = F_{\mathrm{top}} - F_{\mathrm{bot}}, \quad (9)$$

a definition introduced here, with all fluxes positive downward, so that a negative F_{bot} denotes upward supply into the core from below. The ratio $R_{DB} = A_{core,act}/B_{diff}$ provides a compact diagnostic of the local balance between demand and resolved supply. At equilibrium the core budget reduces to $R_{restore} \approx A_{core,act} - B_{diff}$, so $R_{DB} = 1$ is the restoring-neutral point by construction; it is a budget consequence and not an independently discovered threshold.

2.12 Particle-flux attribution

To quantify where the detritus arriving at the core upper interface was produced, passive tagged detrital tracers labelled by production depth are carried alongside the prognostic field. Because the van Leer limiter is a nonlinear function of the *total* detrital field, tags that computed

https://doi.org/10.5194/egusphere-2026-4927
Preprint. Discussion started: 27 August 2026

their own limiters would not sum to the total flux. The limiter coefficients are therefore diagnosed once per sub-step from the total field and reused unchanged for every tag, which makes the decomposition linear and exactly additive. The decomposition is verified by two criteria fixed in advance: additivity of the tagged fluxes at the interface, and closure of the detritus budget for the sub-domain between 50 m and z_u, both to better than 10^{-10} relative. Method and diagnostics are given in Supplement Section S7 and Table S8. The resulting shares are a linear decomposition of a modelled flux and are not Lagrangian particle histories.

3. Results

3.1 Contrasting oxygen states and fixed diagnostic geometry

The five analysed stations span a wide range of background oxygen conditions (Fig. 1b, Table 1). Under the baseline configuration the annual-mean oxygen minimum ranges from 2.71 mmol m^{-3} at S2, 3.54 mmol m^{-3} at S3 and 4.29 mmol m^{-3} at S4 to 14.37 mmol m^{-3} at S6 and 19.72 mmol m^{-3} at S5. The depth of the minimum also differs, so the fixed diagnostic geometry is station specific (Fig. 1c): the core lies at 170–275 m at S3, S4 and S6, shallower at S2 (155–260 m) and deeper at S5.

Two stations require explicit qualification. At S1 the sub-threshold layer extends to the base of the model domain in every configuration, so its lower boundary cannot be located: the WOA23 oxygen target below 127.5 m is a constant downward extrapolation of the deepest observed level, so the apparent sub-threshold layer there is a property of that fill rather than of the oxygen field (Fig. S8a). No OMZ thickness is reported for S1. At S5 the oxygen minimum spans only 19.2–21.2 mmol m^{-3} across the entire experimental sequence, straddling the 20 mmol m^{-3} level, so whether an OMZ is diagnosed there reflects proximity to the threshold rather than a change of regime (Fig. S8b).

https://doi.org/10.5194/egusphere-2026-4927
Preprint. Discussion started: 27 August 2026

3.2 Particle transport redistributes respiratory demand

Figure 2 shows the response at S3 and S4, the two stations with severely depleted cores and non-euphotic upper layers.

Changing the particle-transport configuration alters both the magnitude and the vertical placement of potential respiratory demand (Fig. 2a, c). In the weak configuration, slow sinking combined with rapid remineralisation concentrates demand at shallow depths and little detritus survives to the core. Moving to the baseline configuration shifts the demand profile downward and increases it throughout the upper layer and the core: integrated core potential demand rises from 0.058 to 0.729 mmol $m^{-2}d^{-1}$ at S3, and from 0.063 to 0.889 mmol $m^{-2}d^{-1}$ at S4.

Realised demand is systematically lower than potential demand, and the gap is largest where oxygen is lowest (shaded band in Fig. 2a, c). The core oxygen limitation factor η ranges over 0.47–0.57 at S3 and 0.53–0.64 at S4, so between roughly one third and one half of the potential respiratory demand is suppressed by low oxygen in these cores. The suppression strengthens as the core becomes more depleted, so η falls monotonically as demand rises.

The redistributed demand alters the oxygen structure (Fig. 2b, d). Between the weak and baseline configurations, annual-mean core oxygen falls from 5.02 to 3.81 mmol m^{-3} at S3 and from 6.63 to 4.96 mmol m^{-3} at S4, and oxygen in the overlying layer falls in step. The reduced contrast across the core upper interface weakens the oxygen gradient there, and the downward diffusive supply falls by 27.5 % at S3 and 28.8 % at S4.

This change follows from altering w_D *and* r_d together, and shows that the two steps contribute comparably, so it is not a sinking-speed response. Because the interface diffusivity is prescribed and unchanged between these experiments, the change in F_{top} follows directly from the altered oxygen gradient; that relationship is the diffusion operator itself and carries no independent information.

https://doi.org/10.5194/egusphere-2026-4927
Preprint. Discussion started: 27 August 2026

3.3 Particle-response pathway and parameter identifiability

Isolating w_D at fixed $r_d = 0.10\ d^{-1}$ reveals that the upper-layer response is not monotonic (Fig. 3a). At S3 and S4 the upper-layer potential demand rises steeply from $w_D = 5$ to $10\ m\ d^{-1}$ and then falls slightly at $w_D = 20\ m\ d^{-1}$, so the highest sampled upper-layer demand occurs at $w_D = 10\ m\ d^{-1}$. With four sampled speeds the turning point is bracketed rather than located, and no smooth optimum is claimed. At low sinking speeds particles are remineralised before reaching the upper layer, whereas at high sinking speeds they transit it too quickly to be remineralised within it. This also explains why the (8, 0.10) configuration has *lower* core demand than the baseline despite a smaller sinking speed, and why calling it a strong-demand case would be incorrect.

The non-monotonic behaviour appears only at S3 and S4. At S5 the upper-layer demand increases and then saturates, sampling the ascending limb alone, so no turning point is identified there.

The diffusive supply mirrors this behaviour (Fig. 3b). Across the fixed-r_d sequences, F_{top} varies inversely with upper-layer potential demand in nine of the ten tested transitions; the single exception is the S5 baseline-to-high step, where the driver itself changes by only 0.5 % and is effectively stationary.

Decomposing the weak-to-baseline change along the sequential path (5, 0.15) → (5, 0.10) → (10, 0.10) shows that the r_d and w_D steps contribute comparably (Fig. 3c): -14.9 % and -14.8 % at S3, and -15.4 % and -15.9 % at S4. These are responses along one tested path and do not constitute a unique causal decomposition, since interaction and order dependence were not evaluated.

The three configurations sharing $w_D/r_d = 100$ produce nearly indistinguishable oxygen states (Fig. 3d). Across a fourfold change in each parameter, the oxygen minimum varies by 0.3 %, realised core demand by 1.0 % and F_{top} by 0.5 %. Within the tested range the oxygen response

https://doi.org/10.5194/egusphere-2026-4927
Preprint. Discussion started: 27 August 2026

is therefore much better constrained by the effective transport-to-remineralisation ratio than by w_D or r_d individually. The agreement is close but not exact, and varies systematically with w_D, consistent with the temperature dependence of r_{eff} preventing an exact ratio law.

3.4 Exact core oxygen budgets

The closed core budgets (Fig. 4, Table 3) show how the demand response is accommodated. In the weak configurations, resolved diffusive supply exceeds respiratory demand at all five stations and the restoring term is negative, removing oxygen from the core. As demand rises to the baseline configuration, the restoring term reverses sign at every station and becomes the largest positive contributor at S2, S3, S4 and S5, while resolved diffusion changes comparatively little. Storage is negligible in every case.

The vertical structure of the resolved supply is consistent across stations. Between 74.1 and 101.1 % of the net resolved diffusive supply enters the core across its upper interface (Table 3, Fig. 4c). The share is highest at S3 and S4, 91.9–101.1 %, and lowest at S6, 74.1–77.9 %, where the deeper and better-ventilated water below the core contributes more. At S4 in the weak configuration the share slightly exceeds 100 % because the lower interface is a small net sink rather than a source; across the five supported stations the lower boundary contributes between -1.1 and +25.9 % of the net (Fig. S8d). Oxygen supplied by resolved vertical diffusion therefore reaches these cores predominantly from above, though not to the same degree at every station.

The budgets close at numerical precision. Across all configurations the residual of Eq. (8) is below 10^{-12} mmol $m^{-2}d^{-1}$, and the direct detritus budget closes to 10^{-16}–10^{-14} relative to its largest term (Fig. S4, Tables S4 and S5). Closure at this level does not itself constrain the physics, but it establishes that the individual terms can be interpreted as the actual increments applied by each operator.

https://doi.org/10.5194/egusphere-2026-4927
Preprint. Discussion started: 27 August 2026

3.5 Oxygen-state dependence and regional scope

The mechanism was tested at all five stations whose forcing supports the diagnostic core. Three responses occur at every one of them: core respiratory demand rises steeply with particle transport, resolved diffusive supply is delivered predominantly across the upper interface, and the closure term reverses sign between the weak and baseline configurations (Fig. 4).

The diffusive response is negative at all five, and its magnitude is bracketed by background oxygen state rather than by the size of the particle perturbation. The weak-to-baseline change in F_{top} is -37.3 % at S2, -28.8 % at S4, -27.5 % at S3, -12.4 % at S5 and -9.3 % at S6, against baseline core oxygen of 3.00, 4.96, 3.81, 20.3 and 17.2 mmol m^{-3}. The larger responses occur in the three oxygen-depleted columns and the smaller ones in the two better oxygenated columns, with S2 both the most depleted station and the one in which the mechanism operates most strongly. The ordering within each group is not monotonic in oxygen: S4 responds slightly more strongly than the more depleted S3, and S5 more strongly than the more depleted S6, so oxygen state brackets the response without setting it. Realised core demand rises by a factor of 8 to 13 across the same change at every station, so the modest diffusive response measures how strongly the rest of the budget buffers a large demand perturbation, not how weakly demand responds.

The oxygen limitation factor lies between 0.43 and 0.64 at the depleted S2, S3 and S4 cores and between 0.81 and 0.85 at the better-oxygenated S5 and S6. These values locate each core on the prescribed limitation curve rather than constituting an independent finding; the sensitivity analysis shows how far they move when the constant defining that curve is changed. The station contrast establishes the spread of positions occupied by five differently ventilated columns under one parameter set.

Two limits on generality should be stated with the result. The geometrically defined upper layer is not the same biogeochemical object at every station: the photosynthetic term is an exact zero in the S2–S6 upper layers but not at S1, whose shallower layer reaches into the euphotic

https://doi.org/10.5194/egusphere-2026-4927
Preprint. Discussion started: 27 August 2026

zone (Fig. S8c). And the fixed layers are reference intervals rather than the instantaneous oxygen minimum of every perturbation: at S4 the weak-configuration annual-mean minimum lies at 362.5 m, outside every layer width tested.

3.6 Robustness to the prescribed physical choices

Four prescribed choices set the core budget most directly and are not constrained within this framework: the vertical diffusivity, the oxygen restoring timescale, the oxygen half-saturation constant K_{O2}, and the width of the diagnostic layer. The weak and baseline configurations were repeated at S3 and S4 across all four, each re-integrated to the same convergence criterion and diagnosed over the subsequent complete model year, except the layer width, which was recomputed from the frozen converged profiles without re-integration (Tables S10, S13 and S14). A fifth test is distinct from these because it alters where a closure acts rather than how strong it is: the vertical extent over which oxygen restoring is applied.

The sign of the response is robust and its amplitude is not. The weak-to-baseline F_{top} response is negative in every case across whole-column diffusivity scaled by 0.5 and 2, τ_{O2} of 180 and 730 d, K_{O2} of 1, 4 and 16 mmol m^{-3}, and diagnostic half-widths of 25, 50 and 75 m. Taken together these span a structural sensitivity envelope of -14.3 to -47.3 %, against -27.5 and -28.8 % in the baseline configuration. This envelope reflects prescribed structural choices of the model and is not a confidence interval, nor an estimate of forcing or observational uncertainty. Resolved diffusive supply remains dominated by the upper interface throughout, with shares of 88.0–101.3 %, values above 100 % arising where the lower interface acts as a small sink. The restoring term reverses sign between the weak and baseline configurations in every one of the perturbed pairs.

The K_{O2} result is the most informative of these, because η is algebraically a function of that constant. Varying K_{O2} over a factor of 16 moves η from 0.226 to 0.874, so the baseline range of 0.47–0.86 is a statement about the assumed half-saturation and not a measured property of

https://doi.org/10.5194/egusphere-2026-4927
Preprint. Discussion started: 27 August 2026

the modelled cores. What survives is the displacement: η falls from the weak to the baseline configuration at every K_{O2} tested, and the F_{top} response stays negative at -31.0, -27.5 and -17.7 % at S3 and -32.4, -28.8 and -19.2 % at S4.

The response is not preserved under one of the tested choices. Oxygen restoring is applied over the full water column in the baseline, so the surface cell is relaxed toward climatological oxygen while the same cell is also gas-exchanged with the atmosphere. Excluding the upper 50 m from restoring leaves the response intact at -20.0 % at S3 and -16.8 % at S4. Excluding the upper 100 m collapses it to -1.2 % at S3 and reverses it to +1.1 % at S4. The core still draws down when demand is redistributed, by 0.75 and 0.69 mmol m^{-3} respectively, but oxygen at the core upper interface falls with it, so the contrast across z_u is no longer reduced: the S4 gradient changes from -0.1506 to -0.1522 mmol m^{-3} m^{-1} between the weak and baseline configurations. The column air–sea flux rises by a factor of 3.8 at S3 when the surface is freed from restoring, confirming that part of the excluded ventilation is relocated into the gas-exchange term rather than removed.

The mechanism reported here therefore operates on a column whose upper 100 m is held near climatological oxygen. Where that constraint is released, the compensating adjustment of the overlying water removes the gradient response. The response therefore requires an externally maintained overlying oxygen reservoir, which is the principal reason the baseline percentage should not be read as an oceanic rate.

3.7 Independent evaluation of the modelled oxygen structure

The mechanism operates through the vertical oxygen structure around the core upper interface, so that structure is what is worth testing against observations. WOA23 cannot serve, being both the initial condition and the restoring target. The evaluation below uses BGC-Argo instead, and nothing in the model was adjusted in response to it.

https://doi.org/10.5194/egusphere-2026-4927
Preprint. Discussion started: 27 August 2026

The comparison uses quality-controlled BGC-Argo profiles (Argo, 2026) carrying oxygen within 200 km of a station between 2010 and 2025, screened on the adjusted oxygen quality flag and binned every 25 m (Fig. 6a). Within that radius S3 is sampled by 361 profiles from 16 floats, S4 by 343 from 7, S2 by 298 from 8 and S5 by 170 from 4. The float count rather than the profile count is the relevant sample size, because a drifting float reports every few days and its profiles are strongly autocorrelated; uncertainties below are therefore obtained by resampling whole floats with replacement. The model side is the annual mean of the diagnostic year of the baseline configuration, interpolated onto the same 25 m grid, and both sides are pooled over all months because the observations span fifteen years while the model is forced by a monthly climatology. S1 is not evaluated for the reasons given has only three profiles within 200 km.

Metrics were also recomputed at 100, 150 and 200 km matchup radii (Table S16). Core-layer oxygen and the depth of the oxygen minimum move little with radius at S3 and S4; the float count, 4 to 16 depending on station, is the binding constraint rather than the profile count.

Before comparing, each observational metric was recomputed along three defensible processing paths that differ only in depth-bin labelling and in whether profiles or monthly means are pooled (Table S15). Below roughly 200 m the paths agree to within 5 %. Between 75 and 150 m, where the oxycline sits, they diverge by up to a factor of three. Metrics were therefore admitted only where that spread is small.

Three comparisons survive. The modelled upper oxycline falls within the same 25 m bin as the observed one at all four evaluated stations. The ordering of core-layer oxygen across stations, S2 poorest and S5 best ventilated, is reproduced by the model and is the same along all three processing paths. And core-layer oxygen at S3 and S4, where the observational estimate is itself stable to 4 and 10 %, agrees with the model to about 1 mmol m^{-3}.

https://doi.org/10.5194/egusphere-2026-4927
Preprint. Discussion started: 27 August 2026

Two comparisons fail, and one metric cannot be evaluated at all. The model is biased high in oxygen everywhere, with modelled core-layer values of 2.96, 3.89, 5.10 and 20.2 mmol m^{-3} at S2, S3, S4 and S5 against observed ranges of 1.7–2.4, 2.9–3.0, 2.8–3.1 and 14.3–18.2, a bias that grows with ventilation. The depth of the oxygen minimum is not reproduced at S4 and S5, where the observed estimate is itself unstable to 26 and 79 % and lies 100–200 m below the modelled depth along the pooled-product path. Most consequentially, *the oxygen gradient at* z_u *cannot be constrained by these data*: across the three processing paths the observed value spans 66 to 150 % of its own mean, so the model gradient is neither reliably stronger nor reliably weaker than observed (Table S15). No skill statement about that gradient is made here.

This bounds what the evaluation establishes. It supports the model's general vertical structure and its station-to-station ordering, and it quantifies an oxygen bias. It does not verify the mechanism, because the quantity the mechanism acts through is exactly the one a 25 m observational grid cannot resolve across a 50 m interface. The observation that would test this study is therefore specific: oxygen profiling at vertical resolution finer than the curvature scale of the oxycline, through the upper core interface of the depleted central and western columns.

3.8 Supporting numerical and attribution diagnostics

Supporting diagnostics are reported in the Supplement: convergence behaviour (Fig. S3), budget closure (Fig. S4), the sinking-scheme benchmark (Fig. S5), the parameter structure and degeneracy (Fig. S6), attribution quality control (Fig. S7) and the regional metric limitations (Fig. S8).

Both pre-declared criteria for the particle-flux attribution pass by four orders of magnitude (Fig. S7a, b, Table S8). On that basis, 19–42 % of the modelled core-top sinking flux is attributed to detritus produced between 50 m and z_u under the frozen-total-D-limiter source-tag decomposition, the share rising as particle transfer weakens. This is a supporting diagnostic: it quantifies where the arriving flux was generated within the model.

https://doi.org/10.5194/egusphere-2026-4927
Preprint. Discussion started: 27 August 2026

The attenuation coordinate $Da_{50\to z_u} = \int r_{eff}/w_D \, dz$ orders the configurations correctly but underpredicts the measured flux survival by a factor of 1.3–1.8 (Table S8), because it describes only the through-flux and omits detritus produced within the interval. It is a useful ordering coordinate rather than a predictive flux law.

4. Discussion

4.1 Particle attenuation and the vertical location of respiratory demand

The response of upper-layer demand to sinking speed is not monotonic. Between $w_D = 5$ and 10 m d^{-1} at fixed remineralisation rate, more material survives to the upper layer and is respired there; beyond about 10 m d^{-1} particles traverse the layer faster than they can be remineralised within it, and the demand imposed there declines even as more organic matter reaches greater depth. Export magnitude and the depth at which respiration occurs are therefore distinct quantities, and neither is a monotonic proxy for the other.

This distinction has direct precedent, and one of those precedents is regional. Al Azhar et al. (2017) attributed the contrast between the Arabian Sea and Bay of Bengal oxygen minimum zones to differences in remineralisation depth, which is essentially the present hypothesis advanced for essentially the present basin at regional scale. The contribution here is therefore not the idea that remineralisation depth matters in the Bay of Bengal. It is the local budget: resolving the vertical redistribution of demand around a shallow, fixed core with every term recorded as the increment its operator applies, which makes it possible to separate potential from realised demand, to attribute the diffusive response to a specific interface, and to establish where that response ceases to hold. More broadly, Kwon et al. (2009) showed that displacing the global remineralisation depth alters the air–sea carbon balance substantially at fixed export production. The present result is the oxygen-budget analogue of that argument, applied locally rather than globally, and it sharpens it in one respect: because the OMZ core is a fixed target only tens of metres below the demand maximum, the relevant quantity is not the

https://doi.org/10.5194/egusphere-2026-4927
Preprint. Discussion started: 27 August 2026

remineralisation depth in absolute terms but its position relative to the oxygen minimum and the oxygen gradient above it. A comparable conclusion was reached for a different transport mechanism by Bianchi et al. (2013), who found that vertically migrating animals intensify oxygen depletion at depth by respiring below the euphotic zone organic matter acquired above it. Active and passive transport differ in almost every other respect, but both cases show that relocating respiration in the vertical alters the oxygen field even when the integrated demand does not change. The agreement across two unrelated transport mechanisms suggests the control is a general property of vertically resolved oxygen budgets rather than a feature of either parameterisation.

The single sinking speed used here is an effective bulk parameter and should not be read as a property of individual particles. Vertical particle distributions emerge from settling acting together with aggregation, fragmentation and grazing on a population spanning a wide range of sizes and densities (Stemmann et al., 2004; Boyd and Trull, 2007), and the attenuation length also varies with temperature (Marsay et al., 2015), which the model represents through the temperature dependence of r_{eff} but not through any change in settling behaviour. The non-monotonic response reported here is therefore a property of the reduced model's attenuation balance. It provides a plausible physical interpretation in terms of the competition between transit time and remineralisation time, but the particular turning point at $w_D \approx 10$ m d^{-1} depends on the choice of a single settling velocity and should not be carried over to the real ocean.

4.2 Oxygen limitation as a prescribed control, and a missing feedback

Two features of the model's oxygen dependence constrain how the results should be read, and both follow from the formulation rather than from the experiments.

The first is that the limitation factor is prescribed. Because realised and conditional potential demand differ only through f_{O_2} and the implicit update, η is a demand-weighted mean of a Michaelis–Menten function whose shape is fixed by the single constant K_{O2}. Changing K_{O2} over

https://doi.org/10.5194/egusphere-2026-4927
Preprint. Discussion started: 27 August 2026

a factor of sixteen moves η from 0.23 to 0.87, so the values reported here describe an assumption as much as a state. What the experiments establish is that the modelled cores move down that curve as demand is redistributed, in the same direction at every constant tested. The corresponding partition of remineralisation onto the denitrifying pathway is reported in the Supplement as a property of the formulation, not as a nitrogen-cycle result: it equals 1-η to within 0.006, carries no low-oxygen threshold, and assigns material to that pathway at oxygen concentrations where observations indicate near-complete inhibition. Nitrite, which Bristow et al. (2017) identify as the limiting quantity in this basin, is not resolved, and no inference about fixed-nitrogen loss is drawn anywhere in this study.

The second is that particle attenuation in this model does not respond to oxygen. The oxic and denitrifying rate coefficients sum to within 1 % of the total remineralisation rate regardless of oxygen concentration, so the attenuation length of the detrital field is independent of the oxygen field. The enhanced preservation of organic matter observed through oxygen minimum zones is therefore absent by construction. That matters more here than in a general biogeochemical model, because the subject of this study is where in the vertical respiration occurs: a real oxygen-dependent preservation would displace respiration deeper as the core is depleted, acting against the redistribution examined here and damping the response. The results isolate the transport control with that feedback switched off.

4.3 Particle demand and resolved diffusive oxygen supply

The chain from particle redistribution to diffusive supply operates entirely through the oxygen field. Increased demand in and above the core lowers oxygen there, reduces the contrast across the core upper interface, and the prescribed diffusion operator converts that reduced contrast into a smaller downward flux. Diffusivity does not respond; only the gradient does. The relation between flux and gradient is the operator itself and carries no independent information, so the result is the change in the oxygen structure, not the flux–gradient relation.

https://doi.org/10.5194/egusphere-2026-4927
Preprint. Discussion started: 27 August 2026

Resolved diffusive supply reaches the core almost entirely across its upper interface, 74.1–101.1 % of the net across the five supported stations, with the lower interface acting as a small sink at S4 in the weak configuration where the share exceeds 100 %. This is a statement about the vertical component only. Oxygen supply to the Bay of Bengal thermocline in the real ocean involves the monsoon current system, seasonal and intraseasonal circulation and mesoscale features (Vinayachandran et al., 2004; Resplandy et al., 2009; Vinayachandran et al., 2013), none of which a one-dimensional framework resolves. The two statements are complementary rather than competing: observational and circulation-resolving work constrains how oxygen arrives in the region, whereas the present analysis quantifies how the local particle field modifies the vertical component of supply once the ambient oxygen structure is altered.

4.4 Identifiability, robustness, and the condition the response requires

Three S3 configurations sharing $w_D/r_d = 100$ produce oxygen states agreeing to 0.3–1.0 % across a fourfold change in each parameter. The system is organised primarily by an effective attenuation length, approximately $L_R \sim w_D/r_{eff}$, rather than by either parameter alone. The agreement is close but not exact and varies systematically with w_D, as expected because r_{eff} is temperature dependent and a constant nominal ratio therefore does not give a constant attenuation length at every depth.

The practical consequence, over this tested S3 range, is a calibration hazard: tuning either parameter against oxygen observations while holding the other fixed would locate an apparent optimum that reflects the imposed constraint rather than a property of the system. Broader identifiability would require additional parameter combinations and stations, which were not run here. Difficulties of this kind, in which biogeochemical models carry more adjustable parameters than the available observations can independently determine, have been recognised for some time (Oschlies, 2001; Anderson, 2005). The present result gives a specific and quantified instance for the two parameters that set particle attenuation, in a configuration where

https://doi.org/10.5194/egusphere-2026-4927
Preprint. Discussion started: 27 August 2026

the compensating direction is known in advance rather than inferred from a fit. The evidence is a single triplet at one station, and it constrains the tested range only.

The same caution applies in the opposite direction to the response magnitudes, and more strongly than a single sensitivity pair would suggest. Across perturbations of the vertical diffusivity, the restoring timescale, the oxygen half-saturation constant and the diagnostic layer width, the weak-to-baseline F_{top} response spans -14.3 to -47.3 % against -27.5 and -28.8 % in the baseline configuration. Its sign, the upper-boundary dominance, the suppression of realised demand and the reversal of the restoring term are stable throughout. The percentages are properties of a particular closure configuration and are not transferable model constants; the structural response is what persists across the tested range.

One tested choice bounds that statement, and it changes what may be concluded from the result. When climatological oxygen restoring is excluded from the upper 100 m, the F_{top} response collapses to -1.2 % at S3 and reverses to +1.1 % at S4. The core still draws down, but the oxygen above it falls too, so the contrast across z_u is preserved and the diffusive supply with it. The mechanism diagnosed in this study therefore operates on a column whose upper 100 m is held near the reference climatology. Whether the real Bay of Bengal upper ocean is constrained in an analogous way, by the ventilation pathways that this framework does not resolve, is precisely the question a one-dimensional model cannot answer. Twenty perturbed cases at two stations remain a robustness test, not an uncertainty analysis.

4.5 Comparison with independent oxygen observations

The comparison with BGC-Argo supports the broad vertical oxygen structure of the model and its station ordering, and does not extend beyond that. The upper oxycline falls in the same 25 m bin in model and observations at all four evaluated stations and the ordering of core-layer oxygen is reproduced descriptively. The gradient at z_u is a different matter: it varies by 66 to 150 % of its own mean between defensible processing paths (Table S15), so the available

https://doi.org/10.5194/egusphere-2026-4927
Preprint. Discussion started: 27 August 2026

product does not constrain it. Because the diffusive flux is that gradient multiplied by a prescribed constant, the quantity the mechanism acts through is precisely the one these observations cannot test.

Two disagreements are informative rather than incidental. The observed oxycline at S2 is more than twice as sharp as the modelled one. That is consistent with unresolved lateral or eddy ventilation of the water overlying the core (Vinayachandran et al., 2004; Resplandy et al., 2009; Vinayachandran et al., 2013), but errors associated with the prescribed vertical mixing, the restoring closure, the spatial matchup, climatological pooling and the biological formulation cannot be separated here, so the attribution is not demonstrated. The same disagreement appears in the deep structure at S4 and S5, where the observed minimum lies 100–200 m below the modelled one and the model is biased high in absolute oxygen throughout.

These limitations connect directly to the restoring-depth result. The mechanism requires that the water above the core not deoxygenate with it, and the observations show the real oxygen contrast across the upper interface to be maintained more strongly than the model maintains it locally. That is consistent with the overlying reservoir being externally supplied, which is the condition under which the modelled response survives. A one-dimensional framework cannot demonstrate that the supply is real rather than an artefact of its own closure, and no such claim is made.

The evaluation is also bounded by its own design. The matchup radius is wide, the observations span fifteen years against a climatologically forced model, the vertical resolution is 25 m, and the rank agreement rests on four stations. Table S16 reports how the metrics move between 100, 150 and 200 km and how far resampling whole floats widens them.

4.6 Interpretation of the closure term, model reduction and limitations

The restoring term is the largest positive contributor to the core budget in the higher-demand configurations at S3, S4 and S5, which makes its interpretation consequential. It is the residual

https://doi.org/10.5194/egusphere-2026-4927
Preprint. Discussion started: 27 August 2026

required to close a local budget in a framework that resolves vertical processes and not horizontal ones. It therefore contains unresolved advective and eddy transport, but also any mismatch between the prescribed physics, the biological formulation and the reference climatology toward which the model is relaxed. That mismatch is quantifiable and is reported rather than left implicit: because restoring is linear, the recorded increment gives the annual-mean core offset from the WOA23 target directly as $R_{restore}\ \tau_{O2}/h_{core}$, which agrees with direct integration of target minus model to three significant figures (Table S12). The baseline lies below the WOA23 core-layer target at all five supported stations, with the largest deficits at S2–S4, and every low-w_D configuration lies closer to the climatology than the baseline does. The baseline is the reference parameter configuration for these experiments and was not selected or calibrated by fit to WOA23; because WOA23 is simultaneously the initial condition and the restoring target, closeness to it is not a skill measure, and no configuration is designated as better on that basis.

Those contributions cannot be separated here, and the term is not converted into a lateral oxygen flux, attributed to a named current system, or quoted as a percentage contribution to OMZ maintenance. The ratio R_{DB} organises its sign consistently across the supported stations, but at equilibrium the core budget reduces to $R_{restore} \approx A_{core,act} - B_{diff}$, so a sign change at $R_{DB} = 1$ follows from the budget rather than from any discovered threshold.

Several reductions limit the scope of the results. The physical state is prescribed, so no feedback from biogeochemistry to circulation is represented, and the diffusivity over the entire analysed depth range is a single prescribed constant, 1.0×10^{-5} m^2 s^{-1}, set by the background limb of Eq. (6) rather than by any observational constraint. Every diffusive-flux amplitude reported here scales directly with that number. A second structural assumption acts in the opposite direction to the modelled response: because the oxic and denitrifying pathways sum to within 1 % of the total remineralisation rate regardless of oxygen, particle attenuation length

https://doi.org/10.5194/egusphere-2026-4927
Preprint. Discussion started: 27 August 2026

in this model does not respond to the oxygen field. The enhanced preservation of organic matter observed through oxygen minimum zones is therefore absent by construction, and including it would tend to move respiration deeper as the core is depleted, partly offsetting the mechanism examined here. The particle field is represented by one settling velocity, which compresses the size- and density-dependent behaviour of natural aggregates into a single effective parameter (Stemmann et al., 2004; Boyd and Trull, 2007); the model can therefore describe how the attenuation balance shifts, but not how the underlying particle population would reorganise. The nitrogen cycle is simplified, and nitrite is not resolved, which is the quantity Bristow et al. (2017) identify as limiting in this basin. Five stations do not constitute basin-scale coverage, and their fixed diagnostic layers are reference intervals rather than the instantaneous oxygen-minimum layer of every perturbation: at S4 the weak-configuration annual-mean oxygen minimum lies at 362.5 m, outside every layer width tested. At S1 the uniform 1000 m domain is not supported by either forcing product below 125 m, so S1 is retained only as a forcing-limited contextual and numerical-diagnostic case.

WOA23 is used for initialisation and as the restoring target, so agreement with it is partly imposed and it cannot serve as validation; the independent evaluation uses BGC-Argo instead (Johnson et al., 2009; Riser et al., 2016; Claustre et al., 2020). What remains genuinely outstanding is the closure term itself. Constraining it would require an independent estimate of horizontal oxygen convergence, or a circulation-resolving framework in which that convergence is computed rather than parameterised, and the restoring-depth result shows that this is not a peripheral refinement: it determines whether the diffusive response exists at all.

5. Conclusions

Particle transport sets not only how much organic matter is respired below the euphotic zone but where that respiration occurs, and in a shallow oxygen minimum zone the two are not interchangeable. Raising the detrital sinking speed at fixed remineralisation rate first increases

https://doi.org/10.5194/egusphere-2026-4927
Preprint. Discussion started: 27 August 2026

and then decreases the demand imposed on the layer overlying the core, because particles eventually cross that layer faster than they are remineralised within it. Moving from the weak-transfer to the baseline attenuation configuration increases realised core demand eightfold to thirteenfold and deoxygenates every column whose forcing supports the diagnostic core. The accompanying loss of oxygen contrast across the core upper interface reduces the model-resolved downward diffusive supply at all five of those stations, by -37 to -9 %, with the larger responses in the three oxygen-depleted columns.

The direction of that reduction is robust and its magnitude is not. At the two central stations the sign survives perturbations of the vertical diffusivity, the restoring timescale, the oxygen half-saturation constant and the width of the diagnostic layer, over which the response spans -14 to -48 %. It does not survive freeing the upper 100 m of the column from climatological oxygen restoring: the response then collapses to near zero at one station and reverses sign at the other, because the water above the core deoxygenates with it and the interface contrast is preserved. The negative diffusive response therefore requires that the overlying oxygen reservoir remain externally maintained. What this study identifies is a local, conditional coupling between respiratory demand and the vertical oxygen gradient, not a basin-scale ventilation mechanism, and the oxygen limitation factor that accompanies it is a diagnostic of an assumed half-saturation constant rather than a measured property of the modelled cores.

Two limits bound the result. At S3, configurations sharing a constant ratio of sinking speed to remineralisation rate produce oxygen states differing by about 1 % across a fourfold change in each, so within this tested triplet the oxygen response alone does not uniquely distinguish the two parameters. And independent oxygen profiles support the modelled vertical structure without testing the mechanism: the modelled oxycline falls within one 25 m bin of the observed one and the station ordering of core oxygen is reproduced, but the gradient at the core upper interface, the quantity through which the entire response acts, varies by more than a factor of

https://doi.org/10.5194/egusphere-2026-4927
Preprint. Discussion started: 27 August 2026

two between defensible processing choices and is therefore not constrained by these data. Testing this mechanism observationally requires oxygen profiling finer than the curvature scale of the oxycline through the upper core interface.

Code and data availability

The model is BoB-OMZ1D v1.0.0. The model code, the frozen diagnostic archive from which every figure and table in this paper is generated, and the scripts that produce them will be deposited in a public repository with a persistent identifier before publication [REPOSITORY URL AND SOFTWARE DOI TO BE ASSIGNED]. All figures and tables are generated from the archive by script; no numerical value in this paper was transcribed by hand. The archive records the model version, the git commit and the diagnostic protocol for every case.

All input data are third-party and openly available. Temperature, salinity, dissolved oxygen and nitrate climatologies are from the World Ocean Atlas 2023 (Locarnini et al., 2024; Reagan et al., 2024; Garcia et al., 2024b; Garcia et al., 2024a), monthly objectively analysed fields on the 1° grid, obtained from the NOAA NCEI THREDDS server (woa23_all_o*mm*_01.nc and woa23_all_n*mm*_01.nc for months *mm* = 01–12). Mixed-layer depth is from the Copernicus Marine GLORYS12 global reanalysis (Lellouche et al., 2021), product GLOBAL_REANALYSIS_001_030, monthly means for 2010–2025. Surface shortwave radiation and 10 m wind speed are from the ERA5 reanalysis (Hersbach et al., 2020), monthly averaged single-level fields obtained from the Copernicus Climate Data Store. The independent evaluation uses delayed-mode BGC-Argo synthetic profiles (Argo, 2026) from the Argo Global Data Assembly Centre, 56 float files retrieved from the Coriolis node against the synthetic-profile index of 18 May 2026; profile counts and float identifiers per station are given in Table S16. Table S9 records how each product enters the model, the interpolation applied and

https://doi.org/10.5194/egusphere-2026-4927
Preprint. Discussion started: 27 August 2026

its known limitations. WOA23 supplies both the initial condition and the restoring target and therefore cannot serve as independent validation.

Author contributions

KEZT: designed the study, developed and verified the model, performed the experiments and data analysis, produced the figures and tables, and wrote the manuscript. SS: contributed to the analysis and to writing first draft. SMMU contributed to writing first draft and to review and editing. TMB contributed to writing first draft and to review and editing. ANU contributed to model development and to the analysis. MAMS contributed to all aspects of the study and supervised the work.

Competing interests

The authors declare no competing interests.

https://doi.org/10.5194/egusphere-2026-4927
Preprint. Discussion started: 27 August 2026

References

Al Azhar, M., Lachkar, Z., Lévy, M., and Smith, K. S.: Oxygen minimum zone contrasts between the Arabian Sea and the Bay of Bengal implied by differences in remineralization depth, Geophysical Research Letters, 44, 11106–11114, https://doi.org/10.1002/2017GL075157, 2017.

Anderson, L. A.: On the hydrogen and oxygen content of marine phytoplankton, Deep-Sea Res. I, 42, 1675–1680, https://doi.org/10.1016/0967-0637(95)00072-E, 1995.

Anderson, T. R.: Plankton functional type modelling: Running before we can walk?, J. Plankton Res., 27, 1073–1081, https://doi.org/10.1093/plankt/fbi076, 2005.

Argo: Argo float data and metadata from Global Data Assembly Centre (Argo GDAC), SEANOE, https://doi.org/10.17882/42182, Argo GDAC, Coriolis node; synthetic-profile index of 18 May 2026, 2026.

Bianchi, D., Galbraith, E. D., Carozza, D. A., Mislan, K. A. S., and Stock, C. A.: Intensification of open-ocean oxygen depletion by vertically migrating animals, Nat. Geosci., 6, 545–548, https://doi.org/10.1038/ngeo1837, 2013.

Boyd, P. W. and Trull, T. W.: Understanding the export of biogenic particles in oceanic waters: Is there consensus?, Prog. Oceanogr., 72, 276–312, https://doi.org/10.1016/j.pocean.2006.10.007, 2007.

Breitburg, D., Levin, L. A., Oschlies, A., Grégoire, M., Chavez, F. P., Conley, D. J., Garçon, V., Gilbert, D., Gutiérrez, D., Isensee, K., Jacinto, G. S., Limburg, K. E., Montes, I., Naqvi, S. W. A., Pitcher, G. C., Rabalais, N. N., Roman, M. R., Rose, K. A., Seibel, B. A., Telszewski, M., Yasuhara, M., and Zhang, J.: Declining oxygen in the global ocean and coastal waters, Science, 359, eaam7240, https://doi.org/10.1126/science.aam7240, 2018.

Bristow, L. A., Callbeck, C. M., Larsen, M., Altabet, M. A., Dekaezemacker, J., Forth, M., Gauns, M., Glud, R. N., Kuypers, M. M. M., Lavik, G., Milucka, J., Naqvi, S. W. A., Pratihary, A., Revsbech, N. P., Thamdrup, B., Treusch, A. H., and Canfield, D. E.: N_2 production rates limited by nitrite availability in the Bay of Bengal oxygen minimum zone, Nat. Geosci., 10, 24–29, https://doi.org/10.1038/ngeo2847, 2017.

Buesseler, K. O., Lamborg, C. H., Boyd, P. W., Lam, P. J., Trull, T. W., Bidigare, R. R., Bishop, J. K. B., Casciotti, K. L., Dehairs, F., Elskens, M., Honda, M., Karl, D. M., Siegel, D. A., Silver, M. W., Steinberg, D. K., Valdes, J., Van Mooy, B., and Wilson, S.: Revisiting carbon flux through the ocean's twilight zone, Science, 316, 567–570, https://doi.org/10.1126/science.1137959, 2007.

Burchard, H., Deleersnijder, E., and Meister, A.: A high-order conservative Patankar-type discretisation for stiff systems of production–destruction equations, Appl. Numer. Math., 47, 1–30, https://doi.org/10.1016/S0168-9274(03)00101-6, 2003.

Claustre, H., Johnson, K. S., and Takeshita, Y.: Observing the global ocean with Biogeochemical-Argo, Annu. Rev. Mar. Sci., 12, 23–48, https://doi.org/10.1146/annurev-marine-010419-010956, 2020.

Codispoti, L. A., Brandes, J. A., Christensen, J. P., Devol, A. H., Naqvi, S. W. A., Paerl, H. W., and Yoshinari, T.: The oceanic fixed nitrogen and nitrous oxide budgets: Moving targets as we enter the anthropocene?, Sci. Mar., 65, 85–105, https://doi.org/10.3989/scimar.2001.65s285, 2001.

Devol, A. H.: Denitrification including anammox, In: Nitrogen in the marine environment, edited by Capone, D. G., Bronk, D. A., Mulholland, M. R., and Carpenter, E. J., pp. 263–301, Academic Press, Burlington, Massachusetts, 2 edn., https://doi.org/10.1016/B978-0-12-372522-6.00006-2, 2008.

DeVries, T., Deutsch, C., Primeau, F., Chang, B., and Devol, A.: Global rates of water-column denitrification derived from nitrogen gas measurements, Nat. Geosci., 5, 547–550, https://doi.org/10.1038/ngeo1515, 2012.

Fasham, M. J. R., Ducklow, H. W., and McKelvie, S. M.: A nitrogen-based model of plankton dynamics in the oceanic mixed layer, J. Mar. Res., 48, 591–639, https://doi.org/10.1357/002224090784984678, 1990.

Garcia, H. E., Bouchard, C., Cross, S. L., Paver, C. R., Wang, Z., Reagan, J. R., Boyer, T. P., Locarnini, R. A., Mishonov, A. V., Baranova, O. K., Seidov, D., and Dukhovskoy, D.: World Ocean Atlas 2023, Volume 4: Dissolved Inorganic Nutrients (phosphate, nitrate, silicate), NOAA Atlas NESDIS 92, NOAA National Centers for Environmental Information, Silver Spring, Maryland, https://doi.org/10.25923/39qw-7j08, 2024a.

Garcia, H. E., Wang, Z., Bouchard, C., Cross, S. L., Paver, C. R., Reagan, J. R., Boyer, T. P., Locarnini, R. A., Mishonov, A. V., Baranova, O. K., Seidov, D., and Dukhovskoy, D.: World Ocean Atlas 2023, Volume 3: Dissolved Oxygen, Apparent Oxygen Utilization, Dissolved Oxygen Saturation and 30-year Climate Normal, NOAA Atlas NESDIS 91, NOAA National Centers for Environmental Information, Silver Spring, Maryland, https://doi.org/10.25923/rb67-ns53, 2024b.

Hersbach, H., Bell, B., Berrisford, P., Hirahara, S., Horányi, A., Muñoz-Sabater, J., Nicolas, J., Peubey, C., Radu, R., Schepers, D., Simmons, A., Soci, C., Abdalla, S., Abellan, X., Balsamo, G., Bechtold, P., Biavati, G.,

https://doi.org/10.5194/egusphere-2026-4927
Preprint. Discussion started: 27 August 2026

Bidlot, J., Bonavita, M., De Chiara, G., Dahlgren, P., Dee, D., Diamantakis, M., Dragani, R., Flemming, J., Forbes, R., Fuentes, M., Geer, A., Haimberger, L., Healy, S., Hogan, R. J., Hólm, E., Janisková, M., Keeley, S., Laloyaux, P., Lopez, P., Lupu, C., Radnoti, G., Rosnay, P. de, Rozum, I., Vamborg, F., Villaume, S., and Thépaut, J.-N.: The ERA5 global reanalysis, Q. J. R. Meteorol. Soc., 146, 1999–2049, https://doi.org/10.1002/qj.3803, 2020.

Johnson, K. S., Berelson, W. M., Boss, E. S., Chase, Z., Claustre, H., Emerson, S. R., Gruber, N., Körtzinger, A., Perry, M. J., and Riser, S. C.: Observing biogeochemical cycles at global scales with profiling floats and gliders: Prospects for a global array, Oceanography, 22, 216–225, https://doi.org/10.5670/oceanog.2009.81, 2009.

Kwon, E. Y., Primeau, F., and Sarmiento, J. L.: The impact of remineralization depth on the air–sea carbon balance, Nat. Geosci., 2, 630–635, https://doi.org/10.1038/ngeo612, 2009.

Lellouche, J.-M., Greiner, E., Le Galloudec, O., Garric, G., Regnier, C., Drevillon, M., Benkiran, M., Testut, C.-E., Bourdalle-Badie, R., Gasparin, F., Hernandez, O., Levier, B., Drillet, Y., Remy, E., and Le Traon, P.-Y.: The Copernicus global 1/12° oceanic and sea ice GLORYS12 reanalysis, Front. Earth Sci., 9, 698876, https://doi.org/10.3389/feart.2021.698876, 2021.

Levin, L. A., Ekau, W., Gooday, A. J., Jorissen, F., Middelburg, J. J., Naqvi, S. W. A., Neira, C., Rabalais, N. N., and Zhang, J.: Effects of natural and human-induced hypoxia on coastal benthos, Biogeosciences, 6, 2063–2098, https://doi.org/10.5194/bg-6-2063-2009, 2009.

Locarnini, R. A., Mishonov, A. V., Baranova, O. K., Reagan, J. R., Boyer, T. P., Seidov, D., Wang, Z., Garcia, H. E., Bouchard, C., Cross, S. L., Paver, C. R., and Dukhovskoy, D.: World Ocean Atlas 2023, Volume 1: Temperature, NOAA Atlas NESDIS 89, NOAA National Centers for Environmental Information, Silver Spring, Maryland, https://doi.org/10.25923/54bh-1613, 2024.

Marsay, C. M., Sanders, R. J., Henson, S. A., Pabortsava, K., Achterberg, E. P., and Lampitt, R. S.: Attenuation of sinking particulate organic carbon flux through the mesopelagic ocean, Proc. Natl. Acad. Sci. USA, 112, 1089–1094, https://doi.org/10.1073/pnas.1415311112, 2015.

Martin, J. H., Knauer, G. A., Karl, D. M., and Broenkow, W. W.: VERTEX: Carbon cycling in the northeast Pacific, Deep-Sea Res., 34, 267–285, https://doi.org/10.1016/0198-0149(87)90086-0, 1987.

Masud-Ul-Alam, M., Khan, Md. A. I., and Turjo, K. E. Z.: Inadequate in situ observations make the northern Bay of Bengal a blind spot for models, Discover Oceans, 3, 33, https://doi.org/10.1007/s44289-026-00148-y, 2026.

Naqvi, S. W. A., Naik, H., Jayakumar, D. A., Shailaja, M. S., and Narvekar, P. V.: Seasonal oxygen deficiency over the western continental shelf of India, In: Past and present water column anoxia, edited by Neretin, L. N., pp. 63–101, Springer, Dordrecht, https://doi.org/10.1007/1-4020-4297-3_04, 2006.

Naqvi, S. W. A., Bange, H. W., Farías, L., Monteiro, P. M. S., Scranton, M. I., and Zhang, J.: Marine hypoxia/anoxia as a source of CH_4 and N_2O, Biogeosciences, 7, 2159–2190, https://doi.org/10.5194/bg-7-2159-2010, 2010.

Oschlies, A.: Model-derived estimates of new production: New results point towards lower values, Deep-Sea Res. II, 48, 2173–2197, https://doi.org/10.1016/S0967-0645(00)00184-3, 2001.

Oschlies, A., Brandt, P., Stramma, L., and Schmidtko, S.: Drivers and mechanisms of ocean deoxygenation, Nat. Geosci., 11, 467–473, https://doi.org/10.1038/s41561-018-0152-2, 2018.

Patankar, S. V.: Numerical heat transfer and fluid flow, Hemisphere Publishing Corporation, Washington, DC, ISBN 978-0-89116-522-4, 1980.

Paulmier, A. and Ruiz-Pino, D.: Oxygen minimum zones (OMZs) in the modern ocean, Prog. Oceanogr., 80, 113–128, https://doi.org/10.1016/j.pocean.2008.08.001, 2009.

Reagan, J. R., Seidov, D., Wang, Z., Dukhovskoy, D., Boyer, T. P., Locarnini, R. A., Baranova, O. K., Mishonov, A. V., Garcia, H. E., Bouchard, C., Cross, S. L., and Paver, C. R.: World Ocean Atlas 2023, Volume 2: Salinity, NOAA Atlas NESDIS 90, NOAA National Centers for Environmental Information, Silver Spring, Maryland, https://doi.org/10.25923/70qt-9574, 2024.

Resplandy, L., Vialard, J., Lévy, M., Aumont, O., and Dandonneau, Y.: Seasonal and intraseasonal biogeochemical variability in the thermocline ridge of the southern Indian Ocean, J. Geophys. Res. Oceans, 114, C07024, https://doi.org/10.1029/2008JC005246, 2009.

Riser, S. C., Freeland, H. J., Roemmich, D., Wijffels, S., Troisi, A., Belbeoch, M., Gilbert, D., Xu, J., Pouliquen, S., Thresher, A., Le Traon, P.-Y., Maze, G., Klein, B., Ravichandran, M., Grant, F., Poulain, P.-M., Suga, T.,

https://doi.org/10.5194/egusphere-2026-4927
Preprint. Discussion started: 27 August 2026

Lim, B., Sterl, A., Sutton, P., Mork, K.-A., Vélez-Belchí, P. J., Ansorge, I., King, B., Turton, J., Baringer, M., and Jayne, S. R.: Fifteen years of ocean observations with the global Argo array, Nat. Clim. Change, 6, 145–153, https://doi.org/10.1038/nclimate2872, 2016.

Schmidtko, S., Stramma, L., and Visbeck, M.: Decline in global oceanic oxygen content during the past five decades, Nature, 542, 335–339, https://doi.org/10.1038/nature21399, 2017.

Sengupta, D., Bharath Raj, G. N., and Shenoi, S. S. C.: Surface freshwater from Bay of Bengal runoff and Irrawaddy river discharge on the Andaman Sea, Geophys. Res. Lett., 33, L22609, https://doi.org/10.1029/2006GL027967, 2006.

Shetye, S. R., Shenoi, S. S. C., Gouveia, A. D., Michael, G. S., Sundar, D., and Nampoothiri, G.: Wind-driven coastal upwelling along the western boundary of the Bay of Bengal during the southwest monsoon, Cont. Shelf Res., 11, 1397–1408, https://doi.org/10.1016/0278-4343(91)90042-5, 1991.

Stemmann, L., Jackson, G. A., and Ianson, D.: A vertical model of particle size distributions and fluxes in the midwater column that includes biological and physical processes, Deep-Sea Res. I, 51, 865–884, https://doi.org/10.1016/j.dsr.2004.03.001, 2004.

Stramma, L., Johnson, G. C., Sprintall, J., and Mohrholz, V.: Expanding oxygen-minimum zones in the tropical oceans, Science, 320, 655–658, https://doi.org/10.1126/science.1153847, 2008.

van Leer, B.: Towards the ultimate conservative difference scheme. II. Monotonicity and conservation combined in a second-order scheme, Journal of Computational Physics, 14, 361–370, https://doi.org/10.1016/0021-9991(74)90019-9, 1974.

Vinayachandran, P. N., Murty, V. S. N., and Ramesh Babu, V.: Observations of barrier layer formation in the Bay of Bengal during summer monsoon, J. Geophys. Res. Oceans, 107, 8099, https://doi.org/10.1029/2001JC000831, 2002.

Vinayachandran, P. N., Chauhan, P., Mohan, M., and Nayak, S.: Biological response of the sea around Sri Lanka to summer monsoon, Geophys. Res. Lett., 31, L01302, https://doi.org/10.1029/2003GL018533, 2004.

Vinayachandran, P. N., Shankar, D., Vernekar, S., Sandeep, K. K., Amol, P., Neema, C. P., and Chatterjee, A.: A summer monsoon pump to keep the Bay of Bengal salty, Geophys. Res. Lett., 40, 1777–1782, https://doi.org/10.1002/grl.50274, 2013.

Wanninkhof, R.: Relationship between wind speed and gas exchange over the ocean, J. Geophys. Res. Oceans, 97, 7373–7382, https://doi.org/10.1029/92JC00188, 1992.

Wanninkhof, R.: Relationship between wind speed and gas exchange over the ocean revisited, Limnol. Oceanogr. Methods, 12, 351–362, https://doi.org/10.4319/lom.2014.12.351, 2014.

Weiss, R. F.: The solubility of nitrogen, oxygen and argon in water and seawater, Deep-Sea Res., 17, 721–735, https://doi.org/10.1016/0011-7471(70)90037-9, 1970.

Wiggert, J. D., Murtugudde, R. G., and Christian, J. R.: Annual ecosystem variability in the tropical Indian Ocean: Results of a coupled bio-physical ocean general circulation model, Deep-Sea Res. II, 53, 644–676, https://doi.org/10.1016/j.dsr2.2006.01.027, 2006.

Table 1. Analysed stations and fixed diagnostic geometry. The core is the converged baseline oxygen-minimum depth ±50 m on fixed grid-cell boundaries, giving a 105 m integrated thickness, and the upper layer is the immediately overlying 50 m; both are held fixed across every particle configuration at that station. z_u is the core upper interface. The support columns give the deepest level at which GLORYS12 temperature (T) and WOA23 oxygen (O_2) carry valid data, rounded to the nearest metre; below it the station input file is filled by constant downward extrapolation. S2–S6 are the quantitative stations. S1 is listed for completeness and is excluded from every quantitative result: 75 m of its 105 m core lies below the deepest supported level, so its core integrals are dominated by fill. Depths in metres, O_2 in mmol m^{-3}.

Stn	Setting	Lat (°N)	Lon (°E)	Upper layer (m)	Core (m)	z_u (m)	z_{min} (m)	O_2min	Support T (m)	Support O_2 (m)
S2	northern slope	18.5	91.0	105.0–155.0	155–260	155.0	207.5	2.73	902	2000
S3	central bay	15.0	88.0	120.0–170.0	170–275	170.0	222.5	3.54	902	2800
S4	western central bay	15.5	84.5	120.0–170.0	170–275	170.0	222.5	4.29	902	3000
S5	southern bay	8.0	87.5	130.0–180.0	180–285	180.0	232.5	19.72	902	3600
S6	Andaman side	13.0	94.0	120.0–170.0	170–275	170.0	222.5	14.37	902	1550
S1†	northern bay, shelf	20.5	89.5	45.0–95.0	95–200	95.0	147.5	10.32	78	125

† Context only: 71% of the S1 core lies below the deepest supported level.

Table 2. Model configuration and particle-transport experiments. (a) Final model settings. (b) Particle-transport configurations; w_D is the detrital sinking speed and r_d the reference remineralisation rate. The configuration (8, 0.10) is termed intermediate-high because its converged core demand is lower than that of the baseline.

(a) Model settings

Setting	Value	Note
Vertical domain	0–1000 m	
Levels N	200	uniform Δz = 5 m, centres 2.5–997.5 m
Physical time step	1 h	
Biological sub-steps	20	per physical step
Calendar	360 d	12 months of 30 d
τ_{O2}	365 d	unresolved external exchange
τ_{NO3}	60 d	
Restoring depth range	full column	$z \geq 0$ m
Background K_z	10^{-5} m² s^{-1}	analytic profile, Eq. (6); this value applies at every depth below 60–70 m, i.e. throughout the analysed layers
Detrital sinking	TVD van Leer	Fig. S5
Vertical diffusion	implicit, tridiagonal	
Convergence rule	automatic	layer O_2, total N, P, Z, D

b) Particle-transport configurations

Case	w_D (m d^{-1})	r_d (d^{-1})	Stations	Purpose
weak	5	0.15	S2, S3, S4, S5, S6 (+S1, context)	weak particle transfer
isolation	5	0.10	S3, S4, S5 (+S1, context)	parameter isolation at fixed r_d
near-neutral	5	0.11	S3, S4	near-neutral demand control
intermediate-high	8	0.10	S3, S4	intermediate transfer
baseline	10	0.10	S2, S3, S4, S5, S6 (+S1, context)	reference configuration
high	20	0.10	S3, S4, S5 (+S1, context)	high particle transfer
ratio-low	5	0.05	S3	constant $w_D/r_d = 100$
ratio-high	20	0.20	S3	constant $w_D/r_d = 100$

Table 3. Core oxygen state and exact online budget for the weak and baseline particle configurations at the five stations whose forcing supports the diagnostic core. A_{core} terms are respiratory oxygen demand integrated over the fixed core: potential is the conditional oxygen-unlimited sink evaluated at the realised detrital field, actual the applied value, and $\eta = A_{core,act}/A_{core,pot}$. $B_{diff} = F_{top} - F_{bot}$ is the net resolved vertical diffusive supply with fluxes positive downward, and $R_{restore}$ is the oxygen restoring / closure term. Units mmol O_2 m^{-2} d^{-1} except O_2 (mmol m^{-3}) and the F_{top} share (%). The share exceeds 100% where the lower interface is a net sink. All stations use the full seven-term identity and every budget closes to better than 10^{-12} mmol O_2 m^{-2} d^{-1}. S1 is excluded: 71% of its integrated core lies below the deepest level at which either forcing product carries data; its values are in Table S3 for completeness only. The high configuration was not run at S2 and S6 and is likewise in Table S3. Numerical companion to Figs. 4 and 5.

Station	Case	O_2min	Core O_2	$A_{core,pot}$	$A_{core,act}$	η	B_{diff}	$R_{restore}$	F_{top} share (%)	ΔF_{top} (%)
S2	weak	3.90	4.38	0.0990	0.0533	0.538	0.0967	-0.0433	91.7	–
	baseline	2.73	3.00	0.9854	0.4215	0.428	0.0674	+0.3541	82.4	-37.3
S3	weak	4.60	5.02	0.0583	0.0335	0.574	0.1018	-0.0683	97.7	–
	baseline	3.54	3.81	0.7291	0.3588	0.492	0.0785	+0.2803	91.9	-27.5
S4	weak	5.68	6.63	0.0631	0.0402	0.638	0.1197	-0.0795	101.1	–
	baseline	4.29	4.96	0.8888	0.4931	0.555	0.0909	+0.4022	94.7	-28.8
S5	weak	21.19	21.92	0.0438	0.0372	0.849	0.1698	-0.1326	91.8	–
	baseline	19.72	20.32	0.5778	0.4831	0.836	0.1565	+0.3267	87.2	-12.4
S6	weak	15.74	18.67	0.0606	0.0500	0.825	0.1979	-0.1479	77.9	–
	baseline	14.37	17.24	0.5588	0.4527	0.810	0.1886	+0.2640	74.1	-9.3

https://doi.org/10.5194/egusphere-2026-4927
Preprint. Discussion started: 27 August 2026

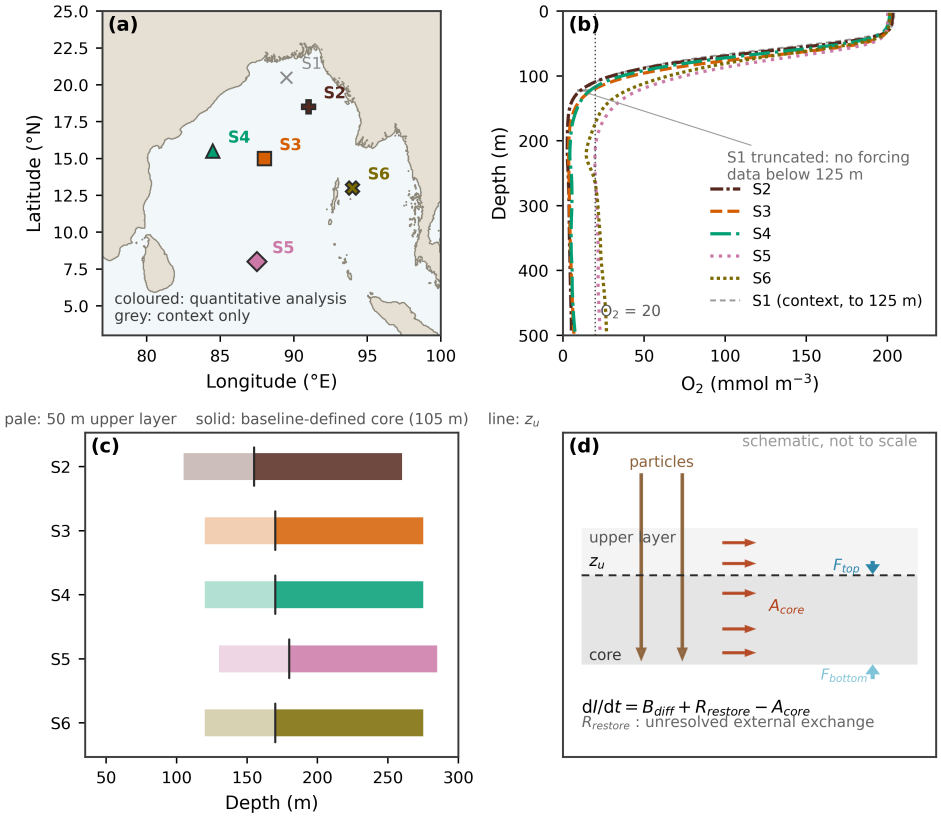

Figure 1. Study setting and diagnostic geometry. (a) Station positions. The five stations whose forcing supports the diagnostic core, S2 to S6, are filled; S1 is marked with a cross and is retained for context only, because 71% of its diagnostic core lies below the deepest level at which either forcing product carries data. Land is shaded. (b) Annual-mean baseline oxygen profiles; the S1 profile is truncated at 125 m, the deepest WOA23 oxygen level at that station. (c) Fixed diagnostic geometry for the five analysed stations: the pale bar is the 50 m upper layer, the solid bar the baseline-defined core (nominally ±50 m about the baseline oxygen minimum, 105 m integrated thickness on the 5 m grid), and the vertical line the core upper interface z_u. Both intervals are defined from that station's converged baseline state and held fixed across every particle-transport configuration. (d) Schematic of the diagnosed balance: detritus sinks and imposes respiratory oxygen demand distributed with depth, while resolved vertical diffusion supplies oxygen across the core interfaces. $R_{restore}$ is the oxygen restoring / closure term; it closes the budget and is not a measured transport. Simulations were integrated until the convergence criterion was satisfied and diagnosed over the subsequent complete 360-day model year.

https://doi.org/10.5194/egusphere-2026-4927
Preprint. Discussion started: 27 August 2026

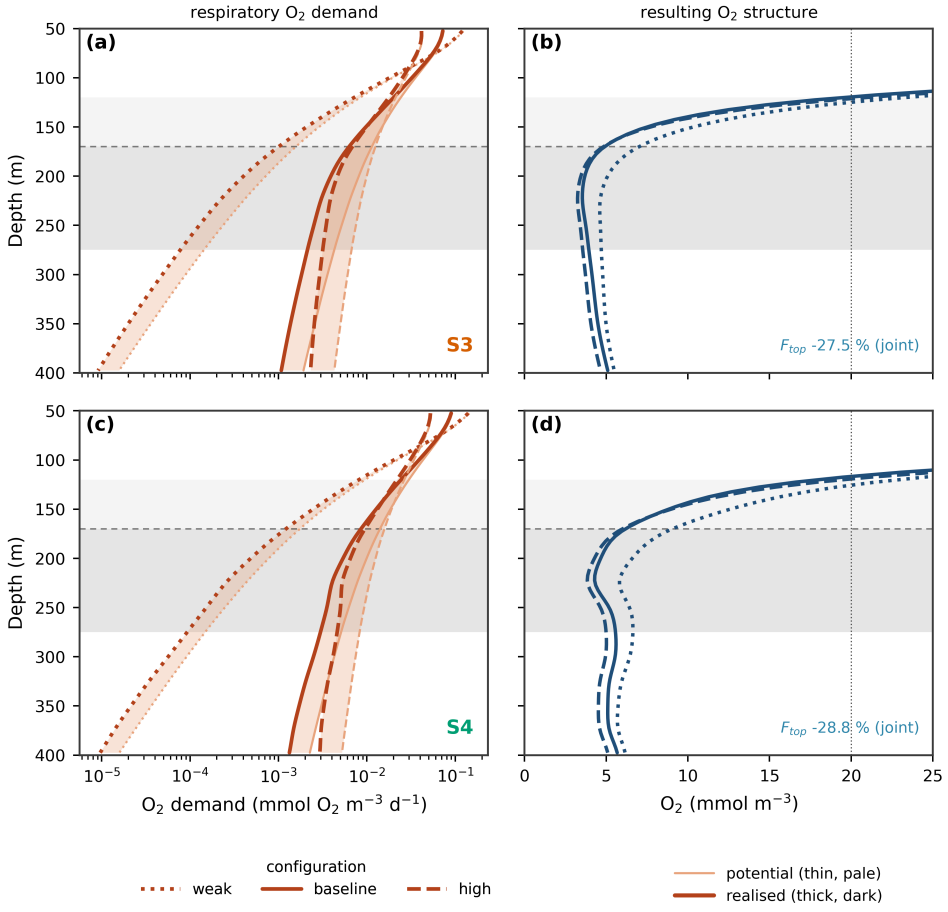

Figure 2. Particle transport redistributes respiratory oxygen demand and alters the oxygen structure of the baseline-defined core layer, at S3 (a, b) and S4 (c, d). Left: conditional potential respiratory demand, the instantaneous oxygen-unlimited sink evaluated at the realised detrital field (thin, pale), and realised demand (thick, dark) for three particle-transport configurations, weak (w_D = 5 m d^{-1}, r_d = 0.15 d^{-1}), baseline (10, 0.10) and high (20, 0.10); the shaded band between them is the prescribed Michaelis–Menten suppression of remineralisation, $f_{O2} = O_2/(K_{O2} + O_2)$ with K_{O2} = 4 mmol m^{-3}, integrated as $\eta = A_{core,act}/A_{core,pot}$ (0.47–0.57 at S3 and 0.53–0.64 at S4). Right: the corresponding annual-mean oxygen. Pale and darker shading mark the fixed upper layer and core; the dashed line is the core upper interface. The annotated change in F_{top}, the downward diffusive oxygen flux across that interface, is the joint response to changing both w_D and r_d between the weak and baseline configurations and is not attributable to sinking speed alone. Its amplitude is specific to this configuration. Because interface diffusivity is prescribed and unchanged among these experiments, changes in F_{top} directly reflect changes in the oxygen gradient. Simulations were integrated until the convergence criterion was satisfied and diagnosed over the subsequent complete 360-day model year.

https://doi.org/10.5194/egusphere-2026-4927
Preprint. Discussion started: 27 August 2026

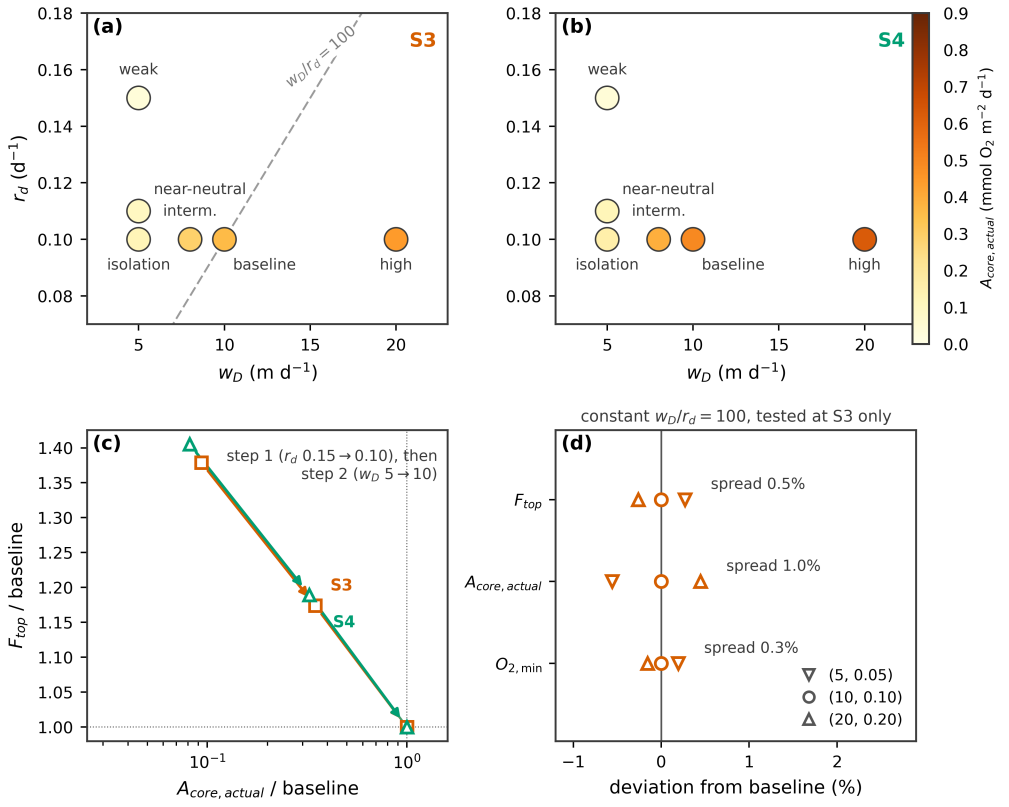

Figure 3. Particle attenuation in parameter space and the limits of parameter identifiability. (a, b) Every configuration actually integrated at S3 and S4 in the (w_D, r_d) plane, with no interpolation between them; fill colour is the realised core respiratory demand $A_{core,actual}$, the dashed line marking constant $w_D/r_d = 100$ is drawn on the S3 panel only, where that triplet was integrated. (c) The same experiments in response space, normalised to the baseline configuration: realised core demand against the core-top diffusive oxygen flux. Arrows follow one sequential isolation path, weak → (5, 0.10) → baseline, in which r_d is changed first and w_D second. This is one ordering of two parameter changes and not a unique causal decomposition; the reverse ordering would attribute the steps differently. (d) Configurations sharing $w_D/r_d = 100$ at S3, as per cent deviation from the baseline. The three quantities agree to within the annotated spreads across a fourfold change in each parameter, so oxygen alone separates the two parameters poorly over this tested triplet. Simulations were integrated until the convergence criterion was satisfied and diagnosed over the subsequent complete 360-day model year.

https://doi.org/10.5194/egusphere-2026-4927
Preprint. Discussion started: 27 August 2026

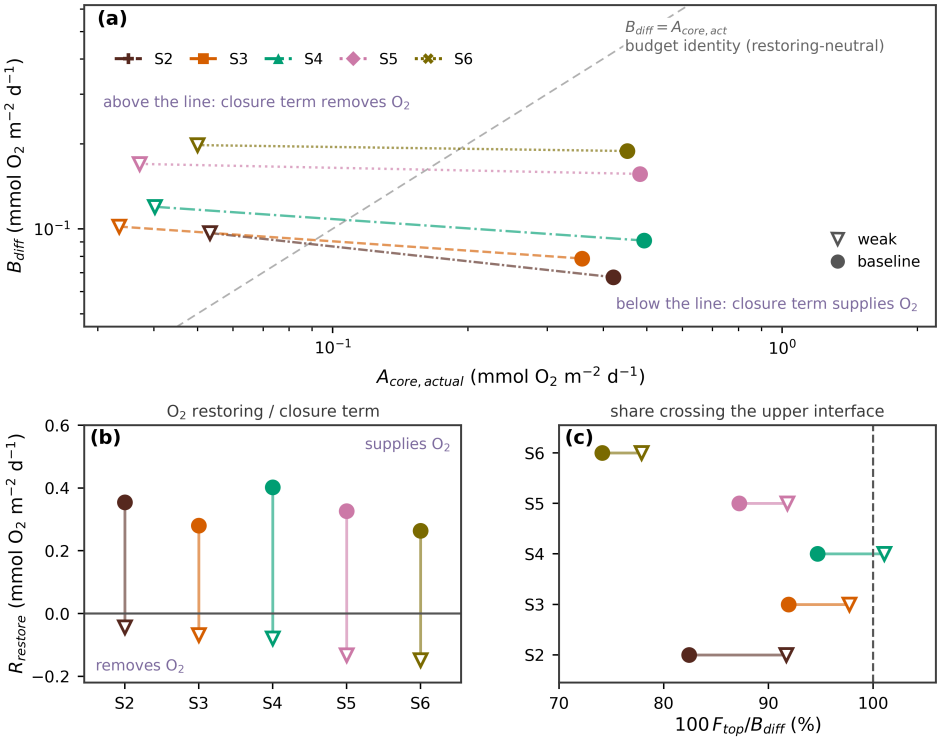

Figure 4. Architecture of the core oxygen budget across the five stations whose forcing supports the diagnostic core. (a) Realised core respiratory demand against resolved diffusive supply, on logarithmic axes because both span more than a decade. The dashed line is the budget identity $B_{diff} = A_{core,actual}$, the restoring-neutral condition under which the closure term vanishes at negligible storage; it is an identity, not a fit or a discovered threshold. Every station moves down and to the right from the weak to the baseline configuration, crossing from the closure term removing oxygen to supplying it. (b) The oxygen restoring / closure term itself. It changes sign between the two configurations at every station. It closes a local vertical budget and cannot be read as a lateral transport. (c) Share of resolved diffusive supply delivered across the core upper interface. Values above 100 per cent occur where the lower interface is a net sink. Simulations were integrated until the convergence criterion was satisfied and diagnosed over the subsequent complete 360-day model year.

https://doi.org/10.5194/egusphere-2026-4927
Preprint. Discussion started: 27 August 2026

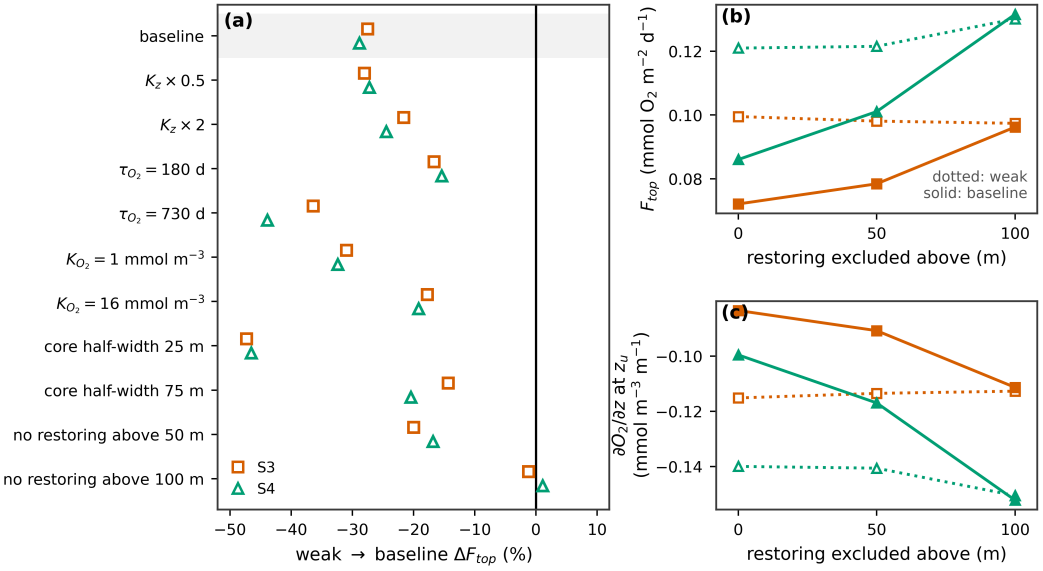

Figure 5. Structural robustness of the diffusive response and the condition under which it fails. (a) Fractional change in the core-top diffusive oxygen flux between the weak and baseline particle configurations, for every perturbation tested. The perturbations tested are prescribed structural choices of the model, not forcing or observational uncertainty. The response is negative across the prescribed diffusivity, the restoring timescale, the oxygen half-saturation constant and the diagnostic layer width, spanning a structural envelope of -14.3 to -47.3 per cent, but it collapses to near zero at S3 and reverses sign at S4 when climatological oxygen restoring is excluded from the upper 100 m. (b) The same experiment shown directly: F_{top} in the weak (dotted) and baseline (solid) configurations as restoring is withdrawn from progressively more of the upper column. The two states converge, and at S4 they cross. (c) The oxygen gradient at the core upper interface. With full-column restoring it weakens substantially between the two configurations; with the upper 100 m free, the water above the core deoxygenates with the core and the gradient contrast is preserved. The mechanism therefore requires that the overlying oxygen reservoir be externally maintained. Simulations were integrated until the convergence criterion was satisfied and diagnosed over the subsequent complete 360-day model year.

https://doi.org/10.5194/egusphere-2026-4927
Preprint. Discussion started: 27 August 2026

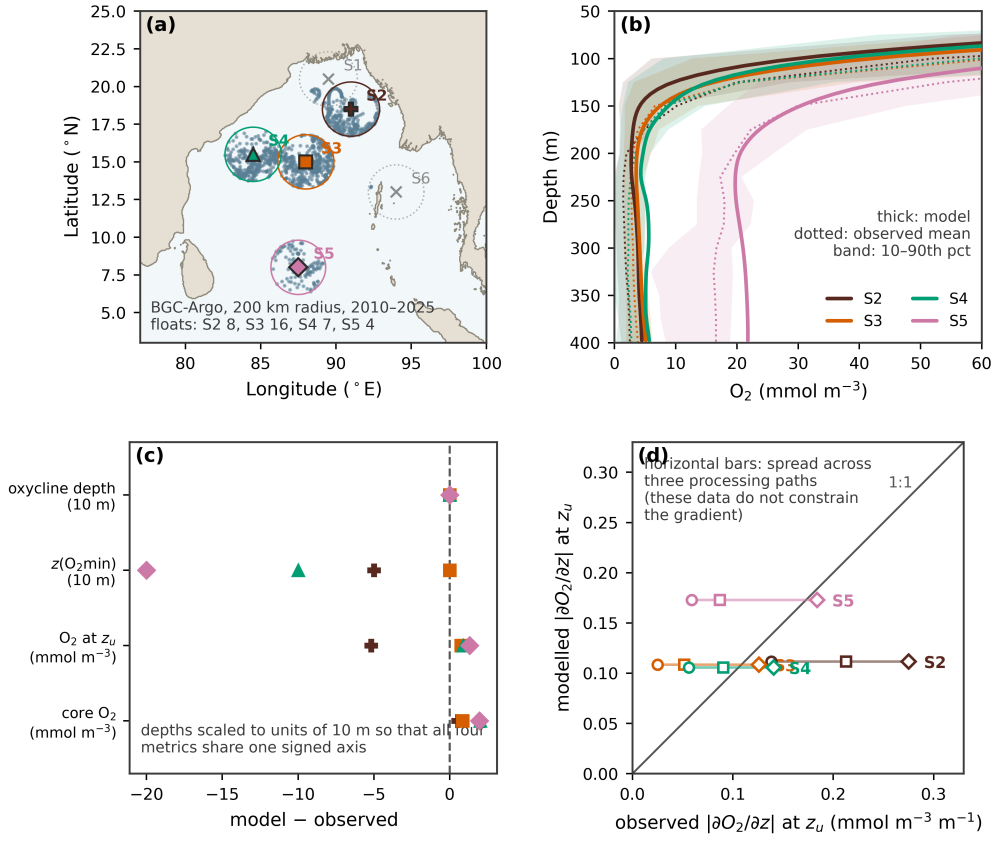

Figure 6. Independent evaluation against BGC-Argo oxygen. No model parameter was adjusted in response to these data, and WOA23 is not used because it is the model's initial condition and restoring target. (a) Quality-controlled BGC-Argo profiles within 200 km of a station, 2010–2025, with the matchup radius drawn. S1 and S6 are marked with crosses and are not evaluated: 71% of the S1 diagnostic core is constant extrapolation and the nearest floats sample materially deeper water, while only three profiles fall within 200 km of S6. (b) Modelled annual-mean oxygen against the observed pooled mean and 10th–90th percentile envelope on the 25 m observational grid. (c) Signed model-minus-observation differences for core-layer oxygen, oxygen at z_u, oxygen-minimum depth and oxycline depth; the two depth differences are plotted in units of 10 m so that all four metrics share one signed axis. The modelled upper oxycline falls within the same 25 m bin as the observed one at all four stations and the ordering of core-layer oxygen is reproduced; the model is biased high in absolute oxygen throughout. (d) The oxygen gradient at the core upper interface. The three symbols per station are three defensible processing paths differing only in depth-bin labelling and pooling; they span 66 to 150% of their own mean, so these data do not constrain the gradient and no agreement is claimed. Simulations were integrated until the convergence criterion was satisfied and diagnosed over the subsequent complete 360-day model year.